

# ReLiCADA - Reservoir Computing using Linear Cellular Automata Design Algorithm

Jonas Kantic , Fabian C. Legl , Walter Stechele , Jakob Hermann 

**Abstract**—In this paper, we present a novel algorithm to optimize the design of Reservoir Computing using Cellular Automata models for time series applications. Besides selecting the models’ hyperparameters, the proposed algorithm particularly solves the open problem of linear Cellular Automaton rule selection. The selection method pre-selects only a few promising candidate rules out of an exponentially growing rule space. When applied to relevant benchmark datasets, the selected rules achieve low errors, with the best rules being among the top 5% of the overall rule space. The algorithm was developed based on mathematical analysis of linear Cellular Automaton properties and is backed by almost one million experiments, adding up to a computational runtime of nearly one year. Comparisons to other state-of-the-art time series models show that the proposed Reservoir Computing using Cellular Automata models have lower computational complexity, at the same time, achieve lower errors. Hence, our approach reduces the time needed for training and hyperparameter optimization by up to several orders of magnitude.

**Index Terms**—Cellular Automata, Dynamical System, Edge of Chaos, Field-Programmable Gate Array, Reservoir Computing, Time Series Prediction.

## I. INTRODUCTION

**R**EAL-time sensor signal processing is a growing demand in our everyday life. High-frequent sensor data is available in a wide range of embedded applications, including, for example, speech recognition, battery protection in electric cars, and monitoring of production facilities. Hence, many application domains could benefit from intelligent and real-time sensor signal analysis on low-cost and low-power devices. To be able to adapt to changing environmental and operational conditions of the target system, machine learning-based approaches have to be employed since classical signal processing techniques often reach their limits under changing external influences. However, at the same time, efficient hardware implementation and acceleration of such intelligent methods are

needed in order to fulfill real-time constraints for applications requiring inference times in the  $\mu$ s to ns range.

Currently, neural network-based models, including Recurrent Neural Networks (RNNs) and Long-Short Term Memorys (LSTMs), form the state-of-the-art for numerous time series processing tasks. However, these models typically consist of several different layers stacked in a deep architecture, have millions of trainable parameters, and include hard-to-implement nonlinear mappings. Such deep architectures are unfavorable for hardware implementations and induce long inference times, which is disadvantageous for real-time applications.

During the last two decades, Reservoir Computing (RC) emerged as a promising alternative to deep and recurrent neural networks. In contrast to the latter, RC models have a shallow architecture and trainable parameters in only a single layer. This makes them generally much easier to design and train. Despite their comparatively simple architecture, RC models have proven their capabilities in many application domains, like biomedical, audio, and social applications [1]. While they only need relatively little computational resources compared to deep neural networks, they still have to be optimized for the unique requirements of, e.g., Field-Programmable Gate Array (FPGA)-based implementations.

Due to the discrete nature of their reservoirs, Reservoir Computing using Cellular Automata (ReCA) models form a subset within the RC framework that is suitable for the implementation on FPGAs. Like for other RC models, the training of ReCA models is easy and fast. Nevertheless, they require extensive hyperparameter tuning.

One major challenge that we address in this paper is that for most ReCA models, the hyperparameter search space is too big for current heuristic search and optimization algorithms. This is especially true for the selection of suitable Cellular Automaton (CA) rules in the reservoir.

Because of this, we conducted the first mathematical analysis of the influence of linear CA rules on the model performance in the ReCA framework and identified common analytical properties of suitable linear rules to be used in the reservoir. We backed our mathematical analysis with the results of almost one million experiments with a sequential runtime of nearly one year using an NVIDIA RTX A4000 GPU (using this GPU, we were able to run three parallel runs of our experiment). In the research community, the ReCA framework has been tested almost solely on pathological datasets that do not allow conclusions about the generality of the conducted studies and generalization capabilities of the ReCA models

This work was supported by the Bavarian Ministry of Economic Affairs, Regional Development and Energy in the context of the Bavarian Collaborative Research Program (BayVFP), funding line Digitization, funding area Information, and Communication Technology. (Jonas Kantic and Fabian Legl contributed equally to this work.) (Corresponding authors: Jonas Kantic and Fabian Legl.)

Jonas Kantic and Walter Stechele are with the Chair of Integrated Systems, Technical University of Munich (TUM), 80333 Munich, Germany (e-mail: jonas.kantic@tum.de, walter.stechele@tum.de).

Fabian Legl and Jakob Hermann are with the Ingenieurbüro für Thermoakustik GmbH (IFTA GmbH), 82178 Puchheim, Germany (e-mail: fabian.legl@tum.de, jakob.hermann@ifta.com)

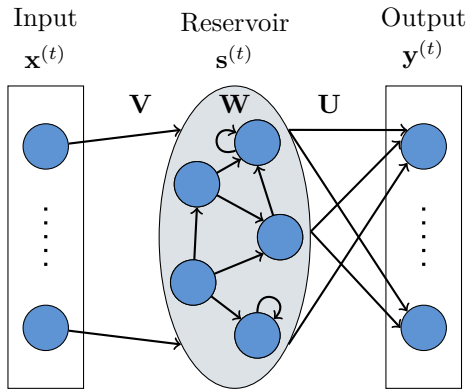


Fig. 1. Echo State Network as an example for Reservoir Computing.

themselves. In the context of this study, we performed an extensive analysis using several benchmark datasets. The result of our research is the Reservoir Computing using Linear Cellular Automata Design Algorithm (ReLiCADA), which specifies Reservoir Computing using Linear Cellular Automata (ReLiCA) models with fixed hyperparameters, and thus immensely simplifies the overall design process. The selected ReLiCA models achieve lower errors than comparable state-of-the-art time series models while maintaining low computational complexity.

The rest of this paper is structured as follows. We first start with an introduction to RC and a review of related work in section II-A, followed by CAs in section II-B, and finally, an overview of the ReCA framework in section II-C. In section II-D, we define the mathematical parameters used in our analysis. After that, we introduce our implementation and refinement of the ReCA model architecture and describe all parts of it in section III. This is followed by an explanation of our novel Reservoir Computing using Linear Cellular Automata Design Algorithm in section IV. The datasets and models that we use to compare and validate our algorithm with are listed in section V, before we analyze the experiments in section VI. The paper is completed by a conclusion in section VII.

## II. BACKGROUND AND RELATED WORK

The in-depth analysis of ReCA models comprises concepts and methods from different research fields, ranging from abstract algebra over automaton theory and properties of dynamical systems to machine learning. In the following sections, we summarize the required background knowledge and related work about RC, CA, and ReCA. Furthermore, we define the mathematical parameters that we use to characterize the ReCA models.

### A. Reservoir Computing

The main idea of RC is to transform the input  $\mathbf{x}$  into a higher dimensional space  $\mathbf{s}$  in order to make the input linearly separable. This transformation is performed by a dynamic system which is called the reservoir (center part of Fig. 1).

The readout layer (right part of Fig. 1) is then used to linearly transform the reservoir state into the desired output  $\mathbf{y}$  [2]. Generally, RC models can be described using

$$\begin{aligned} \mathbf{s}^{(t)} &= g(\mathbf{V}\mathbf{x}^{(t)}, \mathbf{W}\mathbf{s}^{(t-1)}) \\ \mathbf{y}^{(t)} &= h(\mathbf{U}\mathbf{s}^{(t)}) \end{aligned} \quad (1)$$

with the reservoir state  $\mathbf{s}$ , the input  $\mathbf{x}$ , and the output  $\mathbf{y}$  at the discrete time  $t$ . The function  $g$  depends on the reservoir type, while the function  $h$  describes the used readout layer and is typically a linear mapping. During model training, only the output weights  $\mathbf{U}$  are trained, while the input weights  $\mathbf{V}$  and reservoir weights  $\mathbf{W}$  are fixed and usually generated using some model specific constraints. In Fig. 1, we depict an Echo State Network (ESN) [3] using a single layer RNN [4] as the reservoir. Further simplifications to the reservoir were proposed by Rodan et al. [5], resulting in, e.g., the Delay Line Reservoir (DLR) or the Simple Cycle Reservoir (SCR). These types of reservoirs require less computations during the inference step compared to general ESNs. Nevertheless, they are still not suited for implementation in, e.g., FPGAs due to the required floating point calculations. To eliminate the floating point operations in the reservoir, stochastic bitstream neurons can be used [6]. However, stochastic bitstream neurons trade inference speed with the simplicity of implementation on FPGAs and are thus not suited for our usecase [7]. In this paper, we are focusing on a class of RC models that use CAs as the reservoir, which was first proposed by Yilmaz [8] and has been termed ReCA [9]. One of the main advantages of ReCA models compared to other RC models is that the reservoir only uses integer operations on a finite set of possible values. Because of that, they are easy and fast to compute on digital systems like FPGAs.<sup>1</sup>

### B. Cellular Automata

CAs represent one of the simplest types of time, space, and value discrete dynamical systems and have been introduced initially by von Neumann [13], [14]. Following this idea, CAs have been analyzed concerning several different properties, including structural [15], [16], algebraic [17]–[21], dynamical [22]–[26], and behavioral [27]–[31] properties.

The CAs considered in this paper consist of a finite, regular, and one-dimensional lattice of  $N$  cells (see Fig. 2), for reasons discussed later. Each of the cells can be in one of  $m$  discrete states. The lattice is assumed to be circularly closed, resulting in periodic boundary conditions. In this sense, the right neighbor of the rightmost cell ( $s_{N-1}$ ) is the leftmost cell ( $s_0$ ), and vice versa. A configuration of a CA at a discrete iteration<sup>2</sup>  $i$  consists of the states of all its

<sup>1</sup>There are a lot more models inside the RC framework like Liquid State Machine (LSM) [10], Extreme Learning Machine (ELM) [11], Backpropagation-Decorrelation (BPDC) [12], and physical reservoirs [1]. Nonetheless, we will not go into details about them since they are not suitable for our target implementation.

<sup>2</sup>Since the time domain of the CA is different from the time domain of the input data and ReCA model, we will use iterations to describe the CA evolution.

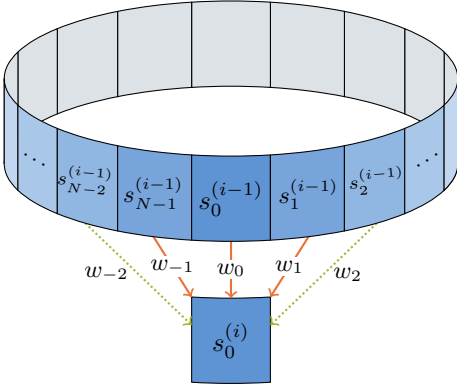


Fig. 2. Lattice of a one-dimensional Cellular Automaton with periodic boundary conditions. Using only the orange weights results in  $n = 3$ ; using the orange and green weights results in  $n = 5$ . The state of the cell  $s_0$  in the  $(i)$ <sup>th</sup> iteration is the weighted sum of the cell states in its neighborhood in the  $(i - 1)$ <sup>th</sup> iteration.

cells at that iteration and can thus be written as a state vector  $\mathbf{s}^{(i)} \in \mathbb{Z}_m^N$  according to

$$\mathbf{s}^{(i)} = (s_0^{(i)}, \dots, s_{N-1}^{(i)}), \quad \text{with } s_k \in \mathbb{Z}_m, \quad (2)$$

where  $\mathbb{Z}_m = \mathbb{Z}/m\mathbb{Z}$  denotes the ring of integers modulo  $m$ , and  $(i)$  denotes the iteration index. The states of each cell change over the iterations according to a predefined rule. At iteration  $(i)$ , the cell state  $s_k^{(i)}$  is defined in dependency of the states of the cells in its neighborhood of fixed size  $n$  at iteration  $(i - 1)$  (see Fig. 2). The neighborhood of a cell contains the cell itself, as well as a range of  $r$  neighboring cells to the left and right, respectively, leading to

$$n = 2r + 1, \quad \text{with } r \in \mathbb{N}^+. \quad (3)$$

We introduce a restriction to the neighborhood  $n$  to define the true neighborhood  $\hat{n}$ . For  $\hat{n}$  we require that  $w_{-r} \neq 0$  or  $w_r \neq 0$ .

The iterative update of the cell states can be described in terms of a local rule  $f: \mathbb{Z}_m^n \rightarrow \mathbb{Z}_m$ , which defines the dynamic behavior of the CA according to

$$s_k^{(i)} = f(s_{k-r}^{(i-1)}, \dots, s_{k+r}^{(i-1)}). \quad (4)$$

Since we use periodic boundary conditions, the indices  $k - r, \dots, k + r$  of the states in (4) have to be taken mod  $N$ .

Linear CAs form a subset of general CAs [21]. The local rule of a linear CA is a linear combination of the cell states in the considered neighborhood. Hence, for linear CAs,  $f$  (see (4)) can be defined as

$$f(s_{k-r}^{(i)}, \dots, s_{k+r}^{(i)}) = \sum_{j=-r}^r w_j s_{k+j}^{(i)} \quad (5)$$

with rule coefficients  $w_j \in \mathbb{Z}_m$ . A linear rule can thus be identified by its rule coefficients  $\mathbf{w} = (w_{-r}, \dots, w_r)$ . Unless otherwise noted, we will restrict the CA rule to linear rules in this paper. A prominent example is the elementary rule 90 CA, which is defined by  $m = 2$ ,  $n = 3$  and  $(w_{-1}, w_0, w_1) = (1, 0, 1)$  [18].

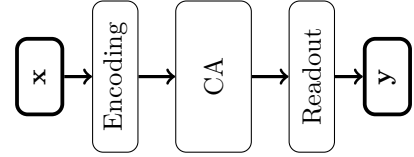


Fig. 3. ReCA architecture as initially proposed by Yilmaz [8]

For each linear rule  $f$ , there exists a mirrored rule  $\hat{f}$  with  $\hat{\mathbf{w}} = (w_r, \dots, w_{-r})$ . If the rule coefficients are symmetric with respect to the central coefficient  $w_0$ , it holds that  $\hat{f} = f$ . In total, there exist  $m^n$  different linear CA rules, which directly follows from (5). We denote the set of all linear rules for given  $m$  and  $n$  by

$$\mathcal{R}(m, n) = \{(w_{-r}, \dots, w_r) : w_i \in \mathbb{Z}_m, n = 2r + 1\}. \quad (6)$$

The local rule  $f$  is applied simultaneously to every cell of the lattice, such that the configuration  $\mathbf{s}^{(i-1)}$  updates to the next iteration  $\mathbf{s}^{(i)}$ , and therefore it induces a global rule  $F: \mathbb{Z}_m^N \rightarrow \mathbb{Z}_m^N$ . For linear CAs, this mapping of configurations can be described by multiplication with a circulant matrix  $\mathbf{W} \in \mathbb{Z}_m^{N \times N}$ , which is given by

$$\mathbf{W} = \text{circ}(w_0, \dots, w_r, 0, \dots, 0, w_{-r}, \dots, w_{-1}), \quad (7)$$

with  $\text{circ}$  as defined in [21] (*note*: if  $N = n$ , the circulant matrix has no additional zero entries that are not rule coefficients). Thus, the global rule for a linear CA can be written as

$$\mathbf{s}^{(i)} = F(\mathbf{s}^{(i-1)}) = \mathbf{W}\mathbf{s}^{(i-1)}. \quad (8)$$

It has been shown that several key properties typically used to characterize dynamical systems are not computable for general CAs. Even for general one-dimensional CAs nilpotency is undecidable, and the topological entropy cannot even be approximated [23], [25], [32]. Furthermore, injectivity and surjectivity can be computed only for one- and two-dimensional CAs [24], [25]. However, when restricting the analysis to one-dimensional linear CAs, all the mentioned properties are computable. This is the reason why we focus on one-dimensional linear CAs in this paper.

### C. ReCA Framework

CAs have been employed as the reservoir in the RC framework first by Yilmaz [8], replacing the recurrently connected neurons typically used in ESNs. The original architecture of a ReCA model is depicted in Fig. 3. Input to the model is a time series  $\mathbf{x}$ , which is fed sample by sample into an encoding stage. The encoding stage, as proposed in [8], serves several purposes. First, the input is preprocessed depending on the type of data, which may include feature expansion, weighted summation, scaling, and binarization. Second, the processed data is mapped to the cells of the CA in the reservoir. Third, the processed data is encoded into the mapped cell states [8]. With the input encoded into its cell states, the global rule of the CA is executed iteratively for a fixed number of iterations.

The output of the CA is then passed to the readout layer, which produces the final model output  $\mathbf{y}$ .

The ReCA framework has been analyzed and developed further based on the initially proposed architecture. In Nichele et al. [33], the authors use hybrid CA-based reservoirs split into two halves, each half running with a different rule to enrich the dynamics within the reservoir. However, this increases the search space for suitable rule combinations in the reservoir, and it remains unclear how to design the reservoir effectively. Deep reservoir computing using the ReCA approach is investigated by Nichele et al. [34] by stacking two ReCA models one after the other, resulting in decreased error rates in most of the analyzed cases. This design principle, however, is to some point contradictory to the original intention of RC, which is to reduce the complexity of supervised training of Neural Networks (NNs) [35]. The analysis of suitable CA rules has been extended from elementary CAs ( $m = 2, \hat{n} = 3$ ) to complex CAs ( $m \geq 3$  and/or  $\hat{n} \geq 5$ ) in [36]. In their work, the authors use a Genetic Algorithm (GA) to perform a heuristic optimization within the super-exponentially growing rule space ( $m^{\hat{n}}$ , since they do not restrict on linear CAs) to find suitable rules for use in the reservoir. One of the biggest challenges with this approach is that the rule space quickly becomes unmanageable for heuristic optimization methods, including genetic algorithms. Even when the number of possible states is only doubled from, e.g.,  $m = 2$  to only  $m = 4$ , the number of possible rules with a three-neighborhood grows from  $2^{2^3} = 256$  to  $4^{4^3} \approx 3.4 \times 10^{38}$ . This example impressively shows that even small increases in complexity of the CA reservoirs make applying heuristic search and optimization methods practically impossible.

Most of the research mentioned above has been mainly based on the synthetic 5-bit and 20-bit memory tasks [8]. However, as the authors in [37] point out, especially the 5-bit memory task is not sufficient to make conclusions about the generalization capability of a model since this task consists of only 32 examples. Furthermore, the model is trained and tested on the whole dataset which contradicts common practice of separating training and test sets. Therefore, they adapt the 5-bit memory task by splitting the 32 examples into a training and test set. This, however, shrinks the number of available train and test examples further. The authors also investigate the effect of different feature extraction techniques on the reservoir output with the result that simply overwriting CA cells in the reservoir works well in less complex CAs.

A rule 90-based FPGA implementation of a ReCA model for the application of handwritten digit recognition based on the MNIST dataset is presented in [38]. Even though their implementation does not reach the classification accuracy of current state-of-the-art Convolutional Neural Network (CNN)-based implementations, the authors show that ReCA is a promising alternative to traditional neural network-based machine learning approaches. This is especially underlined by the fact that the energy efficiency of their implementation is improved by a factor

of 15 compared to CNN implementations [38].

An analysis of the influence of several hyperparameters in the ReCA framework has been conducted in [39], with the result that for general CAs, the overall performance of the model is dependent on and sensitive to the concrete choice of hyperparameters.

#### D. Mathematical Parameters

This section introduces the mathematical parameters we use to analyze linear CA rules. Depending on  $m$ ,  $\mathbb{Z}_m$  is a finite field if  $m$  is prime or otherwise a finite ring. This has several mathematical effects, e.g., the existence of unique multiplicative inverses. Unless otherwise noted, we assume the more general case where  $m$  is not prime ( $\mathbb{Z}_m$  is a ring).

We define the prime factor decomposition of  $m$  as

$$m = p_1^{k_1} \cdots p_h^{k_h} \quad (9)$$

with the set of prime factors as

$$\mathcal{P} = \{p_1, \dots, p_h\} \quad (10)$$

and their multiplicities

$$\mathcal{K} = \{k_1, \dots, k_h\}. \quad (11)$$

The set of prime weights can be generated using

$$\mathcal{P}_w = \{s : \gcd(s, m) = 1\} \quad \forall s \in \mathbb{Z}_m \setminus 0 \quad (12)$$

and the set of non-prime weights by using

$$\bar{\mathcal{P}}_w = \{s : \gcd(s, m) \neq 1\} \quad \forall s \in \mathbb{Z}_m \setminus 0 \quad (13)$$

where  $\gcd$  denotes the greatest common divisor.

1) *Transient and Cycle Lengths*: The behavior of a CA over time can be separated into a transient phase of length  $k$  and a cyclic phase of length  $c$ . For linear CAs, this can be expressed as

$$\mathbf{W}^k \mathbf{s}^{(0)} = \mathbf{W}^{k+c} \mathbf{s}^{(0)} \quad (14)$$

with the circulant rule matrix  $\mathbf{W}$  and the initial configuration  $\mathbf{s}^{(0)}$  [19], [40]. The decomposition of the state space of a CA into transients and cycles gives further information about its dynamic behavior. A linear CA with no transient phase has no Garden-of-Eden states. Garden-of-Eden states have no predecessors and can thus only appear as initial states, if the CA has a transient phase. On the computation of transient and cycle lengths, we refer the interested reader to [40]–[46]<sup>3</sup>.

2) *Cyclic Subgroup Generation*: A cyclic subgroup is generated by a generator element  $g$ . This generator can be used to generate the multiplicative

$$\mathcal{S}^\times(g) = \{g^0, g^1, g^2, \dots, g^{(m-1)}\} \quad (15)$$

and additive

$$\mathcal{S}^+(g) = \{0, g, 2g, \dots, (m-1)g\} \quad (16)$$

cyclic subgroups [47]–[49].

<sup>3</sup>We would like to thank C. Qureshi for his valuable input on the computation of cycle lengths of linear mappings over finite fields.

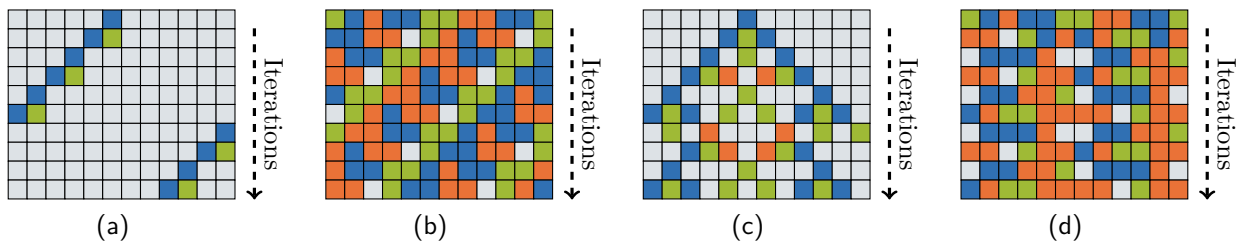


Fig. 4. Iteration diagram of linear CA with  $m = 4$ ,  $\hat{n} = 3$ ,  $N = 12$ ,  $\mathbf{w} = (0, 2, 1)$  (resulting in  $H = 2$ ) and (a) a single cell initialized with state 1 (impulse) or (b) random initial configuration for  $I = 9$  iterations. Figures (c) and (d) have the same setup, but with  $\mathbf{w} = (1, 2, 1)$  (resulting in  $H = 4$ ). The colors indicate different cell states in  $\mathbb{Z}_m$ .

The order of the cyclic additive subgroup  $|\mathcal{S}^+(g)|$  can be calculated by

$$|\mathcal{S}^+(g)| = \frac{m}{\gcd(m, g)} \quad (17)$$

[48], [49]. We use the order of cyclic subgroups to analyze whether the set of possible states during an iteration of a linear CA shrinks or not.

3) *Topological Properties*: For a mathematical analysis, it is often convenient to consider infinite linear CAs whose lattice consist of infinitely many cells [50]. Hence, further properties of infinite one-dimensional CAs can be defined that characterize the behavior of the CA as a dynamic system. For some properties, we only give informal and intuitive descriptions. Formal definitions can be found in [25], [51]–[53]. In the following, the symbol  $\exists_n$  denotes “there exist exactly  $n$ -times”.

a) *State Space and Orbit*: Intuitively, the set of all possible lattice configurations for infinite CAs can be thought of as forming a state space. Furthermore, the notion of distance that induces a metric topology on the state space can be integrated. For a detailed definition, we refer the interested reader to [51]. An individual element in this set is a specific state configuration of the lattice. The series of points in the state space during operation of an infinite linear CA, i.e., the path  $(\mathbf{s}^{(0)}, \dots, \mathbf{s}^{(I)})$  along the visited lattice configurations under iteration of  $F$  for  $I$  iterations with initial configuration  $\mathbf{s}^{(0)}$ , is called orbit. Based on this topological framework, further properties of the dynamic behavior of linear one-dimensional CAs can be computed that characterize it for the asymptotic case of  $N \rightarrow \infty$ . However, only finite lattices can be realized in practical implementations and simulations of CAs, whereby periodic boundary conditions have only limited influence on the behavior of the CA compared to static boundary conditions [54].

b) *Topological Entropy*: The topological entropy is a measure of uncertainty of a dynamical system under repeated application of its mapping function (global rule  $F$  for infinite linear CAs) starting with a partially defined initial state [25]. It can be used to characterize the asymptotic behavior of the system with respect to its operation. Since discrete and finite dynamical systems fall into periodic state patterns, the topological entropy gives an idea of the complexity of the orbit structure and can be used to distinguish ordered and chaotic dynamical

systems. For example, two runs of the same (infinite) linear CA with different initial configurations that are close in the state space can be considered. If the linear CA has a low entropy, the final states of the two runs are also likely to be close in the state space [53]. However, suppose the CA has a high topological entropy. In that case, it shows chaotic behavior and the CA is likely to produce diverging orbits during the two runs even though the initial states were close. Hence, a high entropy leads to increased uncertainty in the dynamical system’s behavior. This behavior can also be seen in Fig. 4, where the orbits of the rule with smaller entropy (Fig. 4a and 4b) show a less chaotic behavior compared to the orbits of the rule with higher entropy (Fig. 4c and 4d).

The topological entropy (probabilistic approach) is closely related to the Lyapunov exponents (geometric approach) and can be computed based thereon. Assuming a CA over  $\mathbb{Z}_m$ , with the prime factor decomposition (9), we define for  $i = 1, \dots, h$

$$\begin{aligned} \mathcal{P}_i &= \{0\} \cup \{j : \gcd(w_j, p_i) = 1\} \\ \mathcal{L}_i &= \min \mathcal{P}_i \\ \mathcal{R}_i &= \max \mathcal{P}_i \end{aligned} \quad (18)$$

with  $w_j$  as defined in (5). Then the left  $\lambda^-$  and right  $\lambda^+$  Lyapunov exponents are [25]

$$\begin{aligned} \lambda^- &= \max_{1 \leq i \leq h} \{\mathcal{R}_i\} \\ \lambda^+ &= - \min_{1 \leq i \leq h} \{\mathcal{L}_i\}. \end{aligned} \quad (19)$$

The topological entropy can be calculated using [25]

$$\mathcal{H} = \sum_{i=1}^h k_i (\mathcal{R}_i - \mathcal{L}_i) \log_2(p_i). \quad (20)$$

To be able to compare the topological entropy of a CA acting on different-sized finite rings, we introduce the normalized topological entropy

$$\tilde{\mathcal{H}} = \frac{\mathcal{H}}{\sum_{i=1}^h k_i \log_2(p_i)} = \frac{\mathcal{H}}{\log_2(m)} \quad (21)$$

with  $m$  as defined in (9). For prime power rings,  $\tilde{\mathcal{H}}$  will only be integer values, where  $\tilde{\mathcal{H}} = 1$  will be the smallest nonzero entropy,  $\tilde{\mathcal{H}} = 2$  the second smallest etc.

c) *Equicontinuity*: A linear CA is said to be *equicontinuous* (or *stable*) if any two states within a fixed size neighborhood in the state space diverge by at most some upper bound distance under iteration of  $F$  [51]. *Equicontinuity* is given if the linear CA fulfills the condition [51]

$$(\forall p \in \mathcal{P}) : p \mid \gcd(m, w_{-r}, \dots, w_{-1}, w_1, \dots, w_r). \quad (22)$$

d) *Sensitivity*: On the other hand, a linear CA is *sensitive* to initial conditions if, for any initial state  $\mathbf{s}^{(0)}$ , there exists another distinct initial state in any arbitrarily small neighborhood of  $\mathbf{s}^{(0)}$ , such that both orbits diverge by at least some lower bound distance [51]. If the condition

$$(\exists p \in \mathcal{P}) : p \nmid \gcd(m, w_{-r}, \dots, w_{-1}, w_1, \dots, w_r) \quad (23)$$

is fulfilled, the corresponding CA is *sensitive* [51].

e) *Expansivity*: Suppose the orbits of any two different states in the state space diverge by at least some lower bound distance under forward iteration of  $F$ . In that case, the corresponding CA is called *positively expansive* [51]. Compared to *sensitivity*, *positive expansivity* is a stronger property. *Positive expansivity* is given for a linear CA if [51]

$$\gcd(m, w_{-r}, \dots, w_{-1}) = \gcd(m, w_1, \dots, w_r) = 1. \quad (24)$$

For invertible infinite linear CAs, this concept can be generalized by additionally considering backward iteration of  $F$  and calling such CAs *expansive* [51]. The condition for *expansivity* is the same as (25) for linear CAs.

f) *Transitivity*: *Transitivity* is given for a linear CA, if it has states that eventually move under iteration of  $F$  from one arbitrarily small neighborhood to any other [52]. In other words, the linear CA cannot be divided into independent subsystems. Codenotti and Margara [55] showed that, for CAs, *transitivity* implies *sensitivity*. The condition for *transitivity* of a linear CA is [52]

$$\gcd(m, w_{-r}, \dots, w_{-1}, w_1, \dots, w_r) = 1. \quad (25)$$

In addition, *strong transitivity* is given if a CA has orbits that include every state of its state space. For *strong transitivity*, a linear CA must fulfill the condition [51]

$$(\forall p \in \mathcal{P})(\exists w_i, w_j) : p \nmid w_i \wedge p \nmid w_j. \quad (26)$$

g) *Ergodicity*: In contrast to *transitivity*, *ergodicity* concerns statistical properties of the orbits of a dynamical system. While *transitivity* indicates the state space of infinite linear CAs cannot be separated, *ergodicity*, intuitively, denotes the fact that typical orbits of almost all initial states (except for a set of points with measure zero) in any subspace under iteration of  $F$  eventually revisit the entire set with respect to the normalized Haar measure [56], [57]. Cattaneo et al. [56] show that, for infinite linear CAs, *ergodicity* and *transitivity* are equivalent. The condition for a linear CA to be *ergodic* is the same as (25).

h) *Regularity*: If cyclic orbits are dense in the state space for an infinite linear CA, then it is denoted as *regular* [52]. *Regularity* is defined for linear CA by condition [52]

$$\gcd(m, w_{-r}, \dots, w_r) = 1. \quad (27)$$

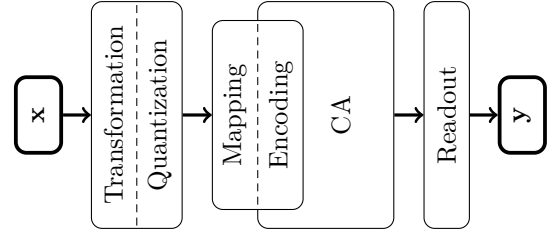


Fig. 5. Refined ReCA architecture

i) *Surjectivity and Injectivity*: The global rule  $F$  of a linear CA is *surjective* if every state configuration has a predecessor. Thus, *surjective* CAs have no Garden-of-Eden states and no transient phase [21]. Cattaneo et al. [56] showed that transitive CAs are surjective. For one-dimensional CAs, *surjectivity* is equivalent to *regularity* of the global rule  $F$  [52]. *Surjectivity* for  $F$  is given if condition (27) is fulfilled [17].

*Injectivity* of  $F$  denotes the fact that every state has at most one predecessor. Every *injective* CA is also *surjective* [51]. If  $F$  is *surjective* and *injective*, the CA is called *bijective*, which is equivalent to reversibility [21]. The condition for *injectivity* of a linear CA is given by [17]

$$(\forall p \in \mathcal{P})(\exists_1 w_i) : p \nmid w_i. \quad (28)$$

j) *Chaos*: The behavior of dynamical systems can range from ordered to chaotic. The framework of dynamical systems lacks a precise and universal definition of chaos. However, there is widespread agreement that chaotic behavior is based on *sensitivity*, *transitivity* and *regularity* [58]. Manzini and Margara [51] identified five classes of increasing degree of chaos for linear CAs: *equicontinuous* CAs, *sensitive* but not *transitive* CAs, *transitive* but not *strongly transitive* CAs, *strongly transitive* but not *positively expansive* CAs, and *positively expansive* CAs. Since for linear CAs, *transitivity* implies *sensitivity* and *surjectivity*, whereby the latter is in turn equivalent to *regularity*, *transitive* linear CAs can be classified as topologically chaotic [56].

4) *Error Metric*: To be able to compare different models, we use the Mean Squared Error (MSE)

$$MSE(\mathbf{y}, \bar{\mathbf{y}}) = \frac{1}{n} \sum_{i=1}^n (\bar{y}_i - y_i)^2 \quad (29)$$

and the Normalized Mean Squared Error (NMSE)

$$NMSE(\mathbf{y}, \bar{\mathbf{y}}) = \frac{MSE(\mathbf{y}, \bar{\mathbf{y}})}{\text{Var}(\bar{\mathbf{y}})} \quad (30)$$

with the ground truth  $\bar{\mathbf{y}}$  and the prediction of the model  $\mathbf{y}$ .

### III. REFINED RECA ARCHITECTURE

Based on the ReCA architecture initially published by Yilmaz [8], we refine our view on the architecture to be able to more precisely define the different computational steps within the ReCA model. In the rest of this paper, without loss of generality, we only consider the

case of one-dimensional time series  $\mathbf{x} = (x^{(0)}, \dots, x^{(T-1)})$  with  $x^{(t)} \in [-1, 1]$ . If n-dimensional data should be used, the transformation, quantization, mapping, and encoding layers are adjusted to the input dimension. For data  $x^{(t)} \notin [-1, 1]$ , the transformation and quantization needs to be adopted.

We split the encoding layer (Fig. 3) into different parts since it fulfills several different and independent tasks. The refined ReCA architecture is depicted in Fig. 5. The input data is fed into the transformation layer (section III-A), which prepares the data for the following quantization. The transformation layer can also be used to run any transformation functions, e.g., tangens hyperbolicus, on the input data. After the input is transformed, we need to quantize it to the allowed states  $x_q \in \mathbb{Z}_m$ . This is done by the quantization layer (section III-B). Note that the transformation and quantization layers often work together to achieve the desired  $x_q$ . The quantized input  $x_q$  is then passed to the mapping layer (section III-C) and then the encoding layer (section III-D). The mapping layer selects the CA cells into which the quantized input should be encoded. The encoding layer then executes the encoding. After the CA in the reservoir updated the cells for a fixed number of iterations, the states of the CA are used by the readout layer (section III-E) to calculate the ReCA model output  $\mathbf{y}^{(t)}$ .

In section III-F, we will combine the aforementioned layers to the ReCA model and describe a complete iteration of the model for an inference time step.

To improve the readability of the definitions, the superscript ( $t$ ) is removed in the rest of this section when the time context is clear.

### A. Transformation

We separate the transformation layer into two steps. First, we apply a transformation function  $\tilde{\mathbf{x}}_\tau = \tau(\mathbf{x})$  to the input. Second, we scale the transformed input to the range  $x_\tau \in [0, m - 1]$  since we require this input range in the subsequent quantization layer. For our setup, we analyzed the following transformation methods:

- *complement*

$$\tilde{x}_\tau = \begin{cases} x, & \text{if } x \in [0, 1], \\ 2 + x, & \text{otherwise.} \end{cases} \quad (31)$$

- *gray* and *scale\_offset*

$$\tilde{x}_\tau = x + 1 \quad (32)$$

- *sign\_value*

$$\tilde{x}_\tau = \begin{cases} x, & \text{if } x \in [0, 1], \\ -x + 1, & \text{otherwise.} \end{cases} \quad (33)$$

Rescaling is then done using

$$x_\tau = \frac{m-1}{2} \tilde{x}_\tau. \quad (34)$$

The idea of the different transformation approaches is to mimic different floating-point to fixed-point conversion

methods. Using the *complement* transformation will represent the numbers similar to a two's complement while *sign\_value* uses a binary sign and value representation. The *scale\_offset* approach will shift the input range to only positive numbers and then use the default binary representation. The *gray* transformation uses the same shift but will encode the values using gray code. The conversion to gray code is only correct if  $m$  is a power-of-two, otherwise neighboring values might not differ in only one bit.

### B. Quantization

To quantize the input values, we use the typical rounding approach

$$\tilde{x}_q = \begin{cases} 0, & \text{if } x_\tau \in [0, 0.5), \\ 1, & \text{if } x_\tau \in [0.5, 1.5), \\ 2, & \text{if } x_\tau \in [1.5, 2.5), \\ \vdots & \\ m-1, & \text{if } x_\tau \in [m-1.5, m-1]. \end{cases} \quad (35)$$

In case of *gray* transformation, the quantized input  $\tilde{x}_q$  is transformed once more, leading to the final quantized value<sup>4</sup>

$$x_q = \begin{cases} \tilde{x}_q \oplus (\tilde{x}_q \gg 1) \bmod m, & \text{if } gray, \\ \tilde{x}_q, & \text{else} \end{cases} \quad (36)$$

with  $\oplus$  representing the binary bitwise *exclusive-or* and  $\gg$  is the binary right-shift operation. The mod  $m$  operation is only needed if  $m$  is not a power of 2.

### C. Mapping

Yilmaz [8] mentions that multiple random projections of the input into the reservoir are necessary to achieve low errors. However, instead of implementing multiple separate CA reservoirs as in [8], we follow the design as described in [36] and subdivide a single CA lattice into multiple parts. Therefore, we divide the lattice of the CA in the reservoir into  $N_r$  compartments. Each compartment has the same number of  $N_c$  cells. For example, a lattice of size  $N = 512$  divided into  $N_r = 16$  compartments with  $N_c = 32$  cells each is described by the tuple  $(N_r, N_c) = (16, 32)$  with  $N = N_r N_c$ . The mapping layer selects the cells of the CA that should receive the input value. One cell is randomly selected out of each compartment, into which the input is encoded in the next step. This random mapping is fixed once and does not change. It can be modeled as a vector  $\mathbf{p} \in \mathbb{Z}_m^N$  with the entries representing the cells of the CA that shall receive the input set to  $x_q$ , and all other entries set to zero (see Fig. 6 part I).

<sup>4</sup>This could also be achieved by changing the quantization function.

#### D. Encoding

Since the mapping layer only defines into which cells the quantized input  $x_q$  should be encoded, we have to define how the encoding is actually done. For this, we use the following commonly used encoding functions. Let  $\bar{s}_0$  be the initial state of an individual cell in the reservoir that has been selected to receive  $x_q$  via random mapping (see section III-C). Then, the encoded cell state  $s_0$  is defined by:

- *replacement* encoding [8]

$$s_0 = x_q \quad (37)$$

- bitwise *xor* encoding [34], [37]

$$s_0 = x_q \oplus \bar{s}_0 \pmod{m}. \quad (38)$$

Note that if  $m$  is a power of two, then the mod  $m$  operation in (38) can be omitted.

Additionally, we analyzed the following new encoding functions:

- *additive* encoding

$$s_0 = x_q + \bar{s}_0 \pmod{m} \quad (39)$$

- *subtractive* encoding

$$s_0 = |x_q - \bar{s}_0| \quad (40)$$

The states of the cells not selected by the mapping layer do not change during the encoding process. The *replacement* encoding overwrites the information stored in the affected cells of the CA with the new input. This is different for the *xor* encoding, which combines the new input with the current cell states and is, next to *replacement* encoding, commonly used in ReCA. In order to analyze the influence of small changes in the encoding, we use the *additive* and *subtractive* encoding schemes, which slightly differ from the *xor* encoding.

#### E. Readout

The readout layer is typically the weighted sum of the reservoir output

$$\mathbf{y} = \mathbf{U}\mathbf{r} + \mathbf{b} \quad (41)$$

with the weight matrix  $\mathbf{U}$  and bias  $\mathbf{b}$ . The reservoir output  $\mathbf{r}$  can be a single state vector  $\mathbf{s}$  of the CA, but is usually chosen to be a concatenation of the CA state at multiple iteration steps [8]. Since  $\mathbf{U}$  and  $\mathbf{b}$  are the only trainable parameter in the ReCA model, a simple linear regression can be used. To simplify the notation, it will be assumed that the input to the readout layer  $\mathbf{r}$  has a 1 appended to also include the bias  $\mathbf{b}$  in the weight matrix  $\mathbf{U}$ .

To train the ReCA model, the reservoir output  $\mathbf{r}^{(t)}$  is concatenated for each input  $\mathbf{x}^{(t)}$  into  $\mathbf{R}$ . Furthermore, the ground truth solutions  $\bar{\mathbf{y}}^{(t)}$  are concatenated in the same way to generate  $\bar{\mathbf{Y}}$ . When using ordinary least squares, the weight matrix  $\mathbf{U}$  can be calculated by

$$\mathbf{U} = (\mathbf{R}^T \mathbf{R})^{-1} \mathbf{R}^T \bar{\mathbf{Y}}. \quad (42)$$

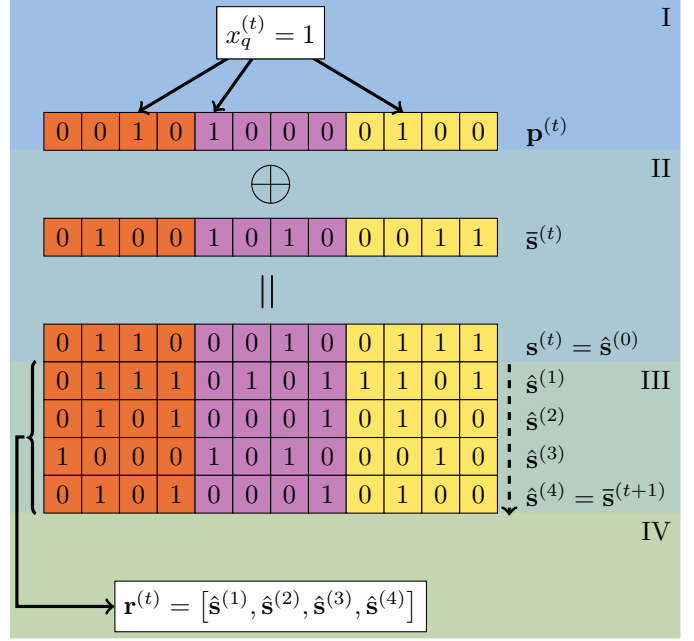


Fig. 6. Example of ReCA computation for an input sample  $x_q^{(t)} = 1$  with an elementary rule 90 CA,  $(N_r, N_c) = (3, 4)$ , *xor* encoding and  $I = 4$  steps. The state of the CA after the  $i^{\text{th}}$  iteration is denoted by  $\hat{\mathbf{s}}^{(i)}$ . The colors of the lattice indicate the three compartments.

There are many different adoptions to the linear regression algorithm. For example, Tikhonov regularization [59], also called L2 regularization, can be added, resulting in Ridge Regression [60]. It is also possible to run linear regression in an online and sequential approach [61]. We use Ridge Regression in our experiments.

#### F. ReCA Computations

For each input sample  $x^{(t)}$ , the ReCA model performs several steps. The whole process is shown for an elementary rule 90 CA [18] and  $I = 4$  iterations in Fig. 6. First, the input is transformed and quantized according to sections III-A and III-B resulting in the quantized sample  $x_q^{(t)}$ . Next,  $x_q^{(t)}$  is mapped to the reservoir cells by the mapping vector  $\mathbf{p}^{(t)}$  as described in section III-C. As an example, Fig. 6 (part I) shows the random mapping of a sample  $x_q^{(t)} = 1$  on the elements of  $\mathbf{p}^{(t)}$ , such that each compartment receives the input at one randomly selected cell. After the mapping, the quantized input has to be encoded into the initial state  $\bar{\mathbf{s}}^{(t)}$  of the reservoir at time  $t$ , resulting in the encoded initial state  $\mathbf{s}^{(t)}$  as described in section III-D. In Fig. 6 (part II), this is depicted for the *xor* encoding. The encoded state  $\mathbf{s}^{(t)}$  forms the initial state  $\hat{\mathbf{s}}^{(0)}$  for the CA, which can then be executed for a fixed number of iterations  $I \in \mathbb{N}^+$ , such that  $\hat{\mathbf{s}}^{(0)}$  evolves under the repeated application of the linear CA rule to  $\hat{\mathbf{s}}^{(I)}$  (see Fig. 6 part III). After the execution of the CA finishes, the reservoir outputs the concatenated CA states  $\mathbf{r}^{(t)} = [\hat{\mathbf{s}}^{(0)}, \dots, \hat{\mathbf{s}}^{(I)}]$  (see Fig. 6 part IV) as mentioned in section III-E. The last state  $\hat{\mathbf{s}}^{(I)}$  will be used as the initial reservoir state  $\bar{\mathbf{s}}^{(t+1)}$  for the next input sample  $x^{(t+1)}$ .



### G. Hyperparameters

Since the trainable parameters in the readout layer can be optimized using simple linear optimization techniques, a crucial step in designing ReCA models is the choice of hyperparameters. In our analysis, we focus on the following general hyperparameters:

- Number of states  $m$  of the CA: This has an influence on the operation domain of the CA since  $\mathbb{Z}_m$  is either a field (if  $m$  is prime) or a ring (if  $m$  is non-prime). It significantly affects the mathematical properties and thus the dynamic behavior of the CA. Since  $m$  defines the number of possible states of each cell, it also influences the linear separability of the reservoir output in the readout layer.
- True neighborhood  $\hat{n}$ : The size of the neighborhood influences the expansion rate of local information on the lattice and thus also affects the dynamic behavior.
- Lattice size  $N$ : This impacts the size of the dynamical system and thus affects the complexity and of the CA
- Subdivision of the lattice into  $N_r$  compartments with  $N_c$  cells each: This influences the mapping of the input samples onto the reservoir cells.
- Number of iterations  $I$  of the CA per input sample: This influences the degree of interactions between the cells per input sample.
- Transformation and quantization: This choice of transformation and quantization functions define how the input data is presented to the dynamical system.
- Mapping and encoding: The mapping and encoding methods define how the input is inserted into the state of the dynamical system.

Next to the general hyperparameters, an increased importance receives the hyperparameter  $F$ , i.e., the global rule of the CA, because it essentially defines the fundamental basis of the dynamics and topological properties of the CA. As the rule space of linear CAs grows exponentially with respect to  $m$  and  $\hat{n}$ , it is vital to receive guidance when it comes to hyperparameter selection in the design process of ReCA models. Since we restrict our analysis to linear rules, we term the respective framework as ReLiCA.

It is important to note that all of these hyperparameters have interdependent effects on the overall behaviour of the CA and in turn on the performance of the ReLiCA model in time series processing tasks.

## IV. PROPOSED RELICA DESIGN ALGORITHM

Since guidance in the choice of hyperparameters would greatly speed-up and assist in the design of ReLiCA models, we propose the Reservoir Computing using Linear Cellular Automata Design Algorithm (ReLiCADA). We start with a short analysis of the influence of the CA rules and transformation, quantization, mapping, and encoding layers on the ReLiCA model performance in section IV-A before introducing our ReLiCADA in section IV-B.

### A. CA Impact on ReLiCA Model Performance

The choice of the CA rule and the choice of transformation, quantization, mapping, and encoding functions sig-

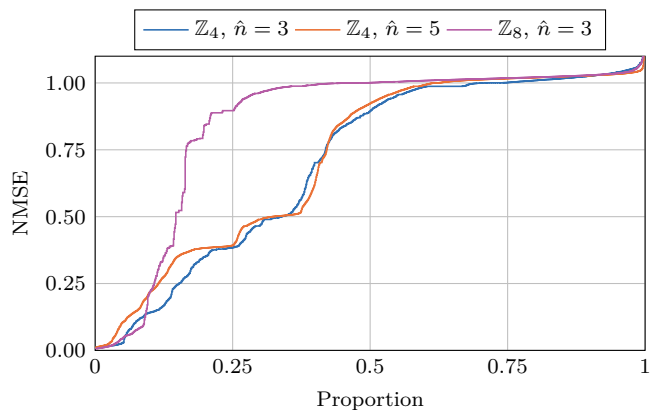


Fig. 7. Empirical cumulative distribution functions for *MG\_25*. The different configurations have the following number of data points: 960, 15360, 8064.

nificantly impact the overall ReLiCA model performance. We depict the *NMSE* for different ReLiCA models for the *MG\_25* dataset (see section V-A) in Fig. 7 (other datasets produce similar results). For this analysis, we ran all possible CA rules with all combinations of the transformation and quantization configurations (*complement*, *gray*, *scale\_offset*, *sign\_value*) and the encoding functions (*additive*, *replacement*, *subtractive*, *xor*). The empirical cumulative distribution function specifies the proportion of ReLiCA models with the same or lower *NMSE*. As the figure shows, only a tiny percentage of all ReLiCA models come close to the optimal performance for the chosen  $m$  and  $\hat{n}$  (lower left part of Fig. 7). To the best of our knowledge, up to date, there are no clear rules or guidelines on how to select the linear CA. Thus, obtaining a well-performing ReLiCA model remained challenging. Because of this, we developed an algorithm that pre-selects promising CA rules. We will introduce this algorithm in the following subsection.

### B. ReLiCA Design Algorithm

We propose the Reservoir Computing using Linear Cellular Automata Design Algorithm (ReLiCADA) to assist in the design of ReLiCA models. ReLiCADA selects combinations of CA rules, transformation, quantization, mapping, and encoding functions that will likely lead to well-performing ReLiCA models. The main idea is to limit the search space of linear CA rules from  $m^n$  (see section II-B) to a small number of promising rules and to select matching transformation, quantization, mapping, and encoding functions. Another purpose of ReLiCADA is to be able to identify ReLiCA models that produce low errors on a wide range of different datasets, and not only on a single pathological dataset like the 5-bit memory task.

ReLiCADA is based on the evaluation of thousands of train-test runs followed by a mathematical analysis of linear CA properties. Our approach was to exhaustively test the performance of ReLiCA models with almost all combinations of the abovementioned transformation, quantization, mapping, and encoding methods over the

complete rule search space of several linear CA configurations ( $\hat{n}$ ,  $m$ ,  $N$  and  $I$ ) on several different datasets. As depicted in Fig. 7, only a tiny percentage of all ReLiCA models achieve low errors, hindering random and heuristic search approaches, especially for complex CAs (larger  $m$  or  $\hat{n}$ ). Our experiments indicate that specific conditions on the choice of the model’s hyperparameters lead to an improvement in performance. For example, some transformation and quantization approaches are more robust against hyperparameter changes than others, and most of the generally good performing linear CA rules share common mathematical properties (see section VI for a detailed discussion of the results of the experiments). We identified these common rule properties and described them in terms of the mathematical parameters as defined in section II-D. The result is ReLiCADA, a set of selection rules, which are applied to the hyperparameters of ReLiCA models. It limits the large number of all possible configurations to a small number of promising candidate models. A crucial part is the pre-selection of only very few linear CA rules that are among the top-performing rules in the overall rule space. In doing so, ReLiCADA enormously reduces the design time of ReLiCA models because it prevents the need to undergo an exhaustive search over the whole linear CA rule space, which is not feasible, especially for more complex CA. Instead, ReLiCADA enables the aimed testing of a few promising models that are sharply defined by the following conditions.

We use the definitions stated in section II-D to describe ReLiCADA. We limited our analysis to  $|\mathcal{P}| \leq 2$ , which will also be assumed in the description of the rule selection algorithm. This was done since we are primarily interested in  $\mathbb{Z}_m$  with a single prime factor. Some of the proposed rules might also work for the case  $|\mathcal{P}| > 2$  or might be generalized, but no verification was done for that.

1) *ReLiCADA Design Rules*: The ReLiCADA selects configurations only if all of the following conditions are fulfilled:

$$\text{transformation} = \text{scale\_offset} \quad (43a)$$

$$\text{quantization} = \text{scale\_offset} \quad (43b)$$

$$\text{mapping} = \text{random} \quad (43c)$$

$$\text{encoding} = \text{replacement} \quad (43d)$$

$$(\forall p \in \mathcal{P})(\exists_1 w_i) : p \nmid w_i \quad (43e)$$

$$\widetilde{\mathcal{H}} = 1 \quad (43f)$$

$$\text{remove mirrored rules} \quad (43g)$$

The following selection rules will only be used based on the choice of  $m$ :

- if  $m$  is not prime, i.e.,  $\mathbb{Z}_m$  forms a ring:

$$\exists_2 i : w_i \neq 0 \quad (44a)$$

$$\forall w_i : (w_i \notin \mathcal{P}_w) \vee (w_i \in \{1, m-1\}) \quad (44b)$$

$$\forall w_i : (w_i \notin \bar{\mathcal{P}}_w) \vee (|\mathcal{S}^+(w_i)| = 4) \quad (44c)$$

- if  $m$  is prime, i.e.,  $\mathbb{Z}_m$  forms a field:

$$\forall w_i : (w_i = 0) \vee (\mathcal{S}^\times(w_i) = \mathbb{Z}_m \setminus 0) \quad (45)$$

- if  $|\mathcal{P}| = 2$ :

$$(\exists w_i, w_j) : (p_1 \nmid w_i) \wedge (p_2 \nmid w_j) \quad (46)$$

Conditions (43) will always be used independent of the choice of  $m$  and  $\hat{n}$ , while conditions (44) to (46) are only used dependent on the choice of  $\mathbb{Z}_m$ . If  $\mathbb{Z}_4$  is chosen, it is impossible to fulfill rule (44c). Because of this, it will be ignored for the  $\mathbb{Z}_4$  case.

The selection (43g) between the rule  $\mathbf{w}$  and its mirrored rule  $\hat{\mathbf{w}}$  is made using the following condition

$$\sum_{i=-r}^{-1} w_i \leq \sum_{i=1}^r w_i, \quad (47)$$

which evaluates to true for only one of the two rules if  $\mathbf{w} \neq \hat{\mathbf{w}}$ . If  $\mathbf{w} = \hat{\mathbf{w}}$ , this condition will always be fulfilled. If the condition is true, we choose  $\mathbf{w}$  and otherwise  $\hat{\mathbf{w}}$ . The selection between  $\mathbf{w}$  and  $\hat{\mathbf{w}}$  is not optimized to increase the performance and is only used to further reduce the number of selected rules. Because of this, also other selection methods between  $\mathbf{w}$  and  $\hat{\mathbf{w}}$  than (47) are possible.

For any given  $N, m$  and  $\hat{n}$ , algorithm 1 implements the process of rule selection (see appendix F).

2) *Reasoning Behind Design Rules*: The conditions (43a) to (43d) fix the transformation, quantization, mapping, and encoding methods to an evidently well-performing combination (see section VI-A). The conditions (43e), (43f) and (44) to (46) belong to the rule selection for the linear CA reservoir. To limit the number of selected rules even further, we added condition (43g).

Our experiments showed that nearly all of the generally well-performing rules are *injective*. Because of this, we included (43e) (see (28)). With this condition, the CA is not only *injective* but also *surjective* and *regular* (see (27)). Moreover, the CAs do not have a transient phase because of the *injectivity* [21]. The *injectivity* of the CA results in them not being *strong transitive* (see (26)) and not being *positive expansive* (see (24)).

Furthermore, it was clear that  $\widetilde{\mathcal{H}}$  has a significant impact on the ReCA model performance. Using (43f) ensures that the CA is *sensitive* (see (23)) as well as *transitive*, *ergodic*, and *expansive* (see (25)). While this would also be the case for other  $\mathcal{H}$  values,  $\widetilde{\mathcal{H}} = 1$  resulted, in most cases, in the best performance and has the advantage of the smallest possible neighborhood  $\hat{n} \geq 3$ , which reduces the complexity of hardware implementations<sup>5</sup>. Condition (43f) also implies that the CA is not *equicontinuous* (see (22)).

Conditions (44) to (46) were chosen to improve the ReCA model performance and reduce the overall amount of rules. These conditions were not chosen based on mathematical characteristics.

3) *Edge of Chaos*: While there is, to the best of our knowledge, no analysis of the Edge of Chaos (EoC) done in the ReCA framework, it is broadly discussed for CAs [28]–[31], [58]. The EoC can be compared to the Edge of

<sup>5</sup>other  $\widetilde{\mathcal{H}}$  values may require  $\hat{n} \geq 5$

TABLE I  
NUMBER OF RULES SELECTED BY ReLiCADA

$\mathbb{Z}_m$	rules selected	total linear rules $\hat{n} = 3$
$m = 3$	1	24
$m = 4$	4	60
$m = 5$	2	120
$m = 6$	2	210
$m = 8$	8	504
$m = 9$	8	720
$m = 12$	8	1716
$m = 16$	8	4080
$m = 32$	8	32736

Lyapunov Stability (EoLS) in the ESNs framework [62]. Verstraeten et.al. [62] analyzed the connection of the Lyapunov exponents of a specific ESN model to its memory and non-linear capabilities. Through these analyses, it was shown that CAs have the highest computational power at the EoC and ESN models at the EoLS.

Using the five groups of CA rules with increasing degree of chaos, as defined by Manzini and Margara [51] (see paragraph II-D3j)), we can see that the CAs selected by ReLiCADA all belong to the third group, implying that they exhibit a “medium” amount of chaos. By the definitions of Devaney and Knudsen they are chaotic, but not expansive chaotic [63]. Since the CA rules selected by ReLiCADA are among the best performing rules, we suppose, without any proof, that this might correlate to the edge of chaos.

As an example, for the configuration  $m = 4$  and  $\hat{n} = 3$ , ReLiCADA selects, among others, the rule with  $\mathbf{w} = (0, 2, 1)$ , which is depicted in Fig. 4a and Fig. 4b. The two iteration diagrams show that this linear CA, on the one hand, has memorization capabilities by shifting the initial state to the left. This left shift can also be interpreted as a transmission of local information along the lattice. On the other hand, it shows interactions of neighboring cells during iteration. These properties (storage, transmission, and interaction) constitute computational capabilities in dynamical systems [29], [31]. Generally, all selected ReLiCADA CA rules show similar behavior.

4) *Number of Rules Selected by ReLiCADA*: In Table I, the number of rules selected by ReLiCADA and the number of all linear rules are listed for different  $m$  and  $\hat{n} = 3$ . It is worth pointing out that the number of selected rules by ReLiCADA is independent of  $\hat{n}$ , whereas the number of total rules depends on the chosen neighborhood  $\hat{n}$ . From Table I, it is easy to see that ReLiCADA reduces the number of rules to analyze by several orders of magnitude. Hence, when designing a ReCA model for a specific application, one does not have to check all rules in the rule space, but only the few rules that are pre-selected by ReLiCADA.

## V. EXPERIMENTS

We will now introduce the experimental setup used to verify and validate the performance of ReLiCADA. The datasets used are introduced in section V-A and the models, to compare the performance of ReLiCADA to, in section V-B.

### A. Datasets

In order to test the performance of the different hyperparameter configurations of the ReLiCA models, we use datasets that have already been used in several other papers to compare different time series models. The following datasets can thus be regarded as benchmark datasets. These datasets might not need fast inference times, one of the main advantages of ReCA models, but are suitable choices for broad comparability with other studies. All datasets are defined over discrete time steps with  $t \in \mathbb{N}$ . We use  $x(t)$  to describe the input to the model, and  $y(t)$  represents the ground truth solution. The  $x$  and  $y$  values are rescaled to  $[-1, 1]$ . Unless otherwise noted, the task is to do a one-step-ahead prediction, i.e.,  $y(t) = x(t + 1)$ , using the inputs up to  $x(t)$ . The abbreviations used to name the datasets throughout the paper are denoted by (*name*).

1) *Hénon Map*: The Hénon Map (*Hénon*) was introduced in [64] and is defined as

$$y(t) = x(t + 1) = 1 - 1.4x(t)^2 + 0.3x(t - 1). \quad (48)$$

2) *Mackey-Glass*: The Mackey-Glass time series uses the nonlinear time-delay differential equation introduced by [65]

$$\frac{dx}{dt} = \beta \frac{x(t - \tau)}{1 + x(t - \tau)^n} - \gamma x(t) \quad (49)$$

with  $\beta = 0.2$ ,  $\gamma = 0.1$ ,  $\tau = 17$ , and  $n = 10$ . The task is to predict  $y(t) = x(t + 1)$  using  $x(t)$  (*MG*). Furthermore, we use the prediction task  $y(t) = x(t + 25)$  using  $x(t)$  (*MG\_25*).

3) *Multiple Superimposed Oscillator*: The Multiple Superimposed Oscillator (*MSO*) is defined as

$$x(t) = \sum_{i=1}^n \sin(\varphi_i t), \text{ with } t \in \mathbb{N}. \quad (50)$$

The MSO12 dataset uses  $\varphi_1 = 0.2$ ,  $\varphi_2 = 0.331$ ,  $\varphi_3 = 0.42$ ,  $\varphi_4 = 0.51$ ,  $\varphi_5 = 0.63$ ,  $\varphi_6 = 0.74$ ,  $\varphi_7 = 0.85$ ,  $\varphi_8 = 0.97$ ,  $\varphi_9 = 1.08$ ,  $\varphi_{10} = 1.19$ ,  $\varphi_{11} = 1.27$ , and  $\varphi_{12} = 1.32$  as defined in [66]. We use the prediction tasks  $y(t) = x(t + 1)$  (*MSO*) and  $y(t) = x(t + 3)$  (*MSO\_3*) with  $x(t)$  as input.

4) *Nonlinear Autoregressive-Moving Average*: The Nonlinear Autoregressive-Moving Average was first introduced in [67] as a time series dataset. We use the 10th order (*NARMA\_10*)

$$x(t + 1) = 0.3x(t) + 0.05x(t) \sum_{i=0}^9 (x(t - i)) + 1.5u(t - 9)u(t) + 0.1, \quad (51)$$

the 20th order (*NARMA\_20*)

$$x(t+1) = \tanh[0.3x(t) + 0.05x(t) \sum_{i=0}^{19} (x(t-i)) + 1.5u(t-19)u(t) + 0.01] + 0.2, \quad (52)$$

and the 30th order (*NARMA\_30*)

$$x(t+1) = 0.2x(t) + 0.004x(t) \sum_{i=0}^{29} (x(t-i)) + 1.5u(t-29)u(t) + 0.201 \quad (53)$$

versions as defined in [68]. The input  $u(t)$  is generated by a uniform independent and identically distributed (i.i.d.) random variable in the interval  $[0, 0.5]$ . The task is to predict  $x(t)$  using  $u(t)$ .

5) *Nonlinear Communication Channel*: This dataset emulates a nonlinear communication channel and was introduced in [69] as

$$\begin{aligned} q(t) &= 0.08u(t+2) - 0.12u(t+1) + u(t) + 0.18u(t-1) \\ &\quad - 0.1u(t-2) + 0.09u(t-3) - 0.05u(t-4) \\ &\quad + 0.04u(t-5) + 0.03u(t-6) + 0.01u(t-7) \\ x(t) &= q(t) + 0.036q(t)^2 - 0.011q(t)^3. \end{aligned} \quad (54)$$

The channel input  $u$  is a random i.i.d. sequence sampled from  $\{-3, -1, 1, 3\}$ . The task is to predict  $x(t-2)$  using  $u(t)$  (*NCC*).

6) *Pseudo Periodic Synthetic Time Series*: Introduced by UC Irvine [70], the dataset can be generated using

$$x(t) = \sum_{i=3}^7 \frac{1}{2^i} \sin \left( 2\pi (2^{2+i} + \text{rand}(2^i)) * \frac{t}{10000} \right) \quad (55)$$

as defined in [71] (*PPST*).

7) *Predictive Modeling Problem*: First introduced by Xue et. al. [72], the dataset can be generated using

$$x(t) = \sin(t + \sin(t)), \quad \text{with } t \in \mathbb{N} \quad (56)$$

(*PMP*).

## B. Compared Models

To have a reference for the ReLiCA model performance values, several state-of-the-art models were used as a baseline. These models and their hyperparameters are established in this section. In the following description, a parameter optimized during hyperparameter optimization is denoted by a range, e.g.,  $[a, b]$ . The results for these models are listed in Table II.

1) *Neural Networks*: These models were created using `TensorFlow 2.8.0` [73] with the default settings unless otherwise noted. The models have an `Input` layer and use a `Dense` layer as output. The hidden layers were adopted to the used model. We used `Adam` [74] as the optimizer, and the learning rate was  $[10^{-10}, 1]$ . As a loss function, *MSE* is used.

The Recurrent Neural Network [4] (*RNN*) uses a `SimpleRNN` layer with 64 units with dropout  $[0, 1]$  and recurrent dropout  $[0, 1]$ .

The `GRU` layer was used for the Gated Recurrent Unit NN [75] with 32 units and dropout  $[0, 1]$ .

The Long Short Term Memory NN [76] uses the `LSTM` layer with 32 units and dropout  $[0, 1]$ .

The Neural Network [77] *NN* model uses  $[1, 4]$  `Dense` layers with  $[1, 64]$  neurons per layer as hidden layers. The inputs to this model are the last 20 values of  $x(t)$ , which results in the vector  $\mathbf{x} = [x(t-19), x(t-18), \dots, x(t)]$ .

2) *RC Models*: We used an ESN, SCR, and DLR model. All models use the `Scikit-learn 1.1.2` [78] Ridge optimizer with an alpha  $[10^{-10}, 1]$ .

The *ESN* model [3] uses the Tensorflow Addons ESN cell implementation embedded into our code. We used 128 units with a connectivity of 10%. The other parameters are input scale  $[0, 10]$ , input offset  $[-10, 10]$ , spectral radius  $[0, 1]$ , and leaky integration rate  $[0, 1]$ .

We implemented the *SCR* and *DLR* models according to [5]. Both use 256 units, a spectral radius of  $[0, 1]$ , input scale  $[0, 10]$ , and input offset  $[-10, 10]$ .

3) *ReCA Models*: We used our implementation of our modified ReCA architecture together with the non-linear CA rules found by a GA in [36]. The lattice has a size of  $(16, 32)$ , and the CA performs four iterations per input sample. All rules found by Babson et al. [36] were analyzed using all combinations of the transformation and quantization configurations (*complement*, *gray*, *scale\_offset*, *sign\_value*) and the encoding functions (*additive*, *replacement*, *subtractive*, *xor*). A Ridge optimizer is used for training. We call this model *Babson*.

The ReCA models were trained using 100 parallel models with 1100 time samples each. For testing and validation, 1100 data points are used. For training, testing, and validation, the first 100 data points are used as initial transient and are not utilized.

4) *Linear Model*: A simple linear regression model using `Scikit-learn` was also evaluated. Like the *NN*, the linear model, denoted by *Linear*, has the last 20 values of  $x(t)$  as input.

5) *Hyperparameter Optimization*: The hyperparameter optimization framework `Optuna` [79] is used to optimize the hyperparameters of the models. We use the `TPE-Sampler` algorithm with 100 runs per model. For models using epoch-based training, early stopping was used. It was configured to stop the training if the loss is not decreasing by at least  $10^{-5}$  with a patience of three epochs.

6) *Complexity*: One of the main advantages of ReCA models is their low computational complexity. To compare the complexities of the different types of models, we approximated their computational complexities of the inference step. This analysis was optimized for implementations on FPGAs without the usage of specialized hardware like multiply-accumulate units. Nevertheless, it should be a good indication also for other types of implementations. Assuming two numbers  $a, b$  that are represented by  $a', b'$  bits, we define the following complexities:

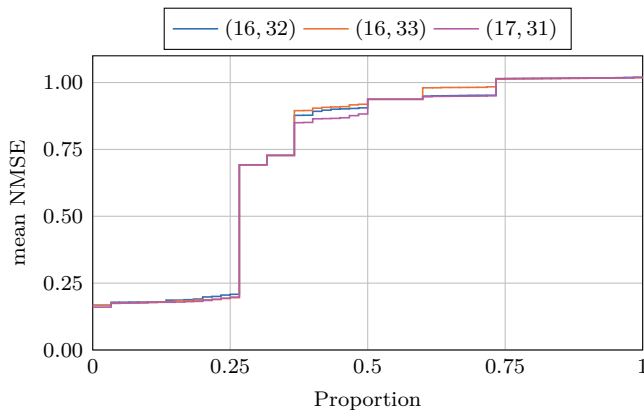


Fig. 8. Influence of the lattice size  $(N_r, N_c)$  on ReLiCA with  $\mathbb{Z}_4$ ,  $\hat{n} = 3$ ,  $I = 4$  `scale_offset`, and `replacement`.

addition and subtraction have a complexity of  $\min(a', b')$ , whereas multiplication and division have a complexity of  $a' \times b'$ . For the additions and subtractions, we assume that the hardware does not need to deal with the most significant bits (MSBs) of the larger number since these are zero in the smaller number. For multiplication and division, we assume a shift-and-add implementation. To approximate the complexity of the *tanh* function, we use the seventh-order Lambert’s continued fraction [80] as an approximation. We assume the same complexity for the *sigmoid* function. The *ReLU* function has a complexity of zero.

We assume that the input and output have 32 bits, and all models use 32 bits to represent their internal states. For the ReCA models, the CA uses the required number of bits to represent  $\mathbb{Z}_m$ , and the readout layer also uses 32 bits.

The number of units in the different baseline models was chosen to make the overall model complexity similar to the tested ReLiCA models. Because of this, the number of units was not optimized for model performance.

## VI. RESULTS

The results of our experiments can be divided into two phases. In the first phase, as described in section VI-A, we identified well-working choices for some of the general hyperparameters of the ReLiCA model that were fixed for the large number of experiments and exhaustive CA rule performance analysis in phase two, which is described in section VI-B. Detailed results of the experiments can be found in appendix C.

### A. General Hyperparameters

Since the main focus of our analysis lies in selecting suitable combinations of transformation, quantization, mapping, and encoding methods, and linear CA rules for the reservoir, we fixed some of the hyperparameters of the ReLiCA framework to reduce the parameter space. Therefore, we first analyzed the influence of the reservoir size  $(N)$  and the number of CA iterations on the overall

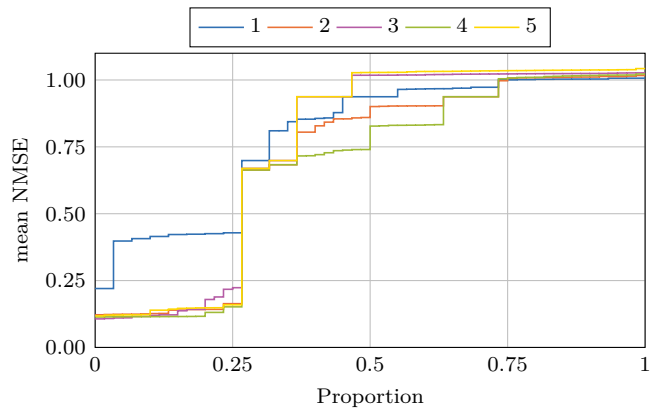


Fig. 9. Influence of the number of iterations  $I$  on ReLiCA with  $\mathbb{Z}_4$ ,  $\hat{n} = 3$ ,  $(16, 32)$ , `scale_offset`, and `replacement`.

ReLiCA performance. The datasets used for the following analysis are MG, MG\_25, MSO, MSO\_3, NARMA\_10, NARMA\_20, NARMA\_30, NCC, PPST, PPST\_10, PMP (see section V-A).

To test the influence of the reservoir size, we tested the following lattice sizes:  $(16, 32)$ ,  $(16, 33)$ , and  $(17, 31)$ . These were chosen since the total number of cells is similar, but their prime factor decomposition differs significantly. The results for the ReLiCA model using `scale_offset`, `replacement`,  $\mathbb{Z}_4$ ,  $\hat{n} = 3$  and  $I = 4$  are depicted in Fig. 8. Other ReLiCA models showed similar behavior. Since none of the lattice sizes is superior to the others, we used  $(16, 32)$  in the following experiments. This was done since, for most hardware implementations, a power-of-two number of cells would most likely be suitable.

To see the influence of the CA iterations we tested the ReLiCA model using `scale_offset`, `replacement`,  $\mathbb{Z}_4$ ,  $\hat{n} = 3$ , and  $(N_r, N_c) = (16, 32)$ . The results are shown in Fig. 9, and other configurations resulted in similar results. Increasing the number of CA iterations to  $> 2$  steps did not lead to a significant monotonic decrease in the overall *NMSE*. This is in line with the results by Babson et al. [36], where they achieved a success rate of 99% in the 5-bit memory task for complex CA reservoirs and four iterations. In their study, elementary ( $m = 2$ ,  $\hat{n} = 3$ ) CAs were found to require eight iterations. However, Nichele et al. [33] show that several single elementary CA rules also achieve a success rate of  $\geq 95\%$  in the 5-bit memory task with only four iterations. Since higher numbers of CA iterations imply a higher computational complexity and longer training and testing times, we fixed the number of iterations to four in all subsequent experiments.

Another finding is that the `replacement` encoding together with the `scale_offset` transformation achieves low errors in most configurations and is thus the most stable encoding with respect to changing values of the other hyperparameters. This can be seen in Fig. 10. Therefore, we fixed the transformation method to `scale_offset` and the encoding to random `replacement`.

The random mapping generator’s seeds, the only random element in the ReLiCA model, were fixed to ensure

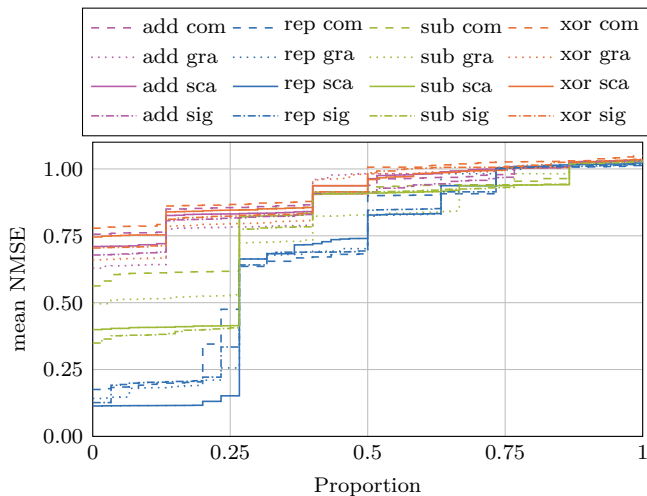


Fig. 10. Comparison of the different transformation, quantization, mapping, and encoding functions using ReLiCA with  $\mathbb{Z}_4$ ,  $\hat{n} = 3$ ,  $I = 4$ ,  $(N_r, N_c) = (16, 32)$ . Used abbreviations: *additive*, *replacement*, *subtractive*, *xor*; *complement*, *gray*, *scale\_offset*, *sign\_value*.

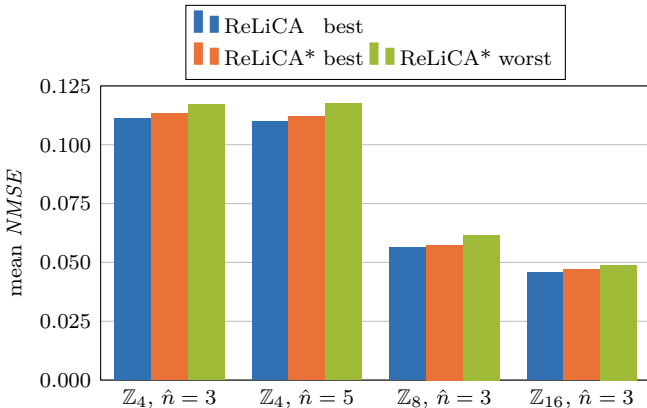


Fig. 11. Comparison of the performance of the overall best linear rule with the best and worst rule selected by ReLiCADA.

reproducible results.

### B. Rule Selection

To analyze the performance of the Reservoir Computing using Linear Cellular Automata Design Algorithm, we used the following time-series benchmark datasets: MG, MG\_25, MSO, MSO\_3, NARMA\_10, NARMA\_20, NARMA\_30, NCC, PPST, PPST\_10, PMP (see section V-A). To train the ReLiCA models, a Ridge optimizer is used with  $\alpha = 1$ , the default value for Scikit-learn. The number of states  $m$ , neighborhood  $\hat{n}$ , and local rule of the CA are varied throughout the experiments. We denote the models designed using ReLiCADA by ReLiCA\* and the general class of ReLiCA models using the whole set of possible linear CA rules by ReLiCA. All individual performance values are listed in the appendices A and C. We used a train-test split for the datasets to conduct our experiments. Unless otherwise noted, the test performance values are used.

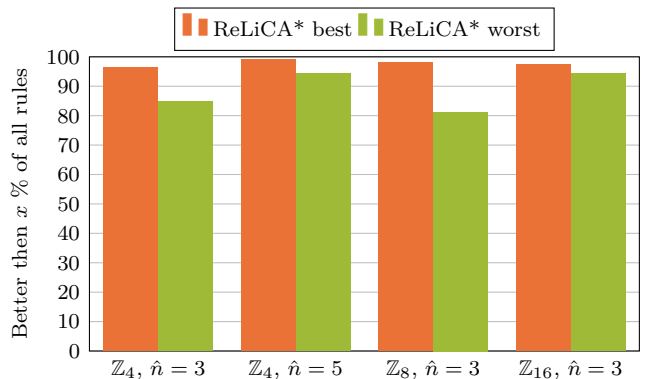


Fig. 12. Rules selected by ReLiCADA are better than  $x\%$  of the overall linear rules.

In Fig. 11, we compare the mean  $NMSE$  of the overall best ReLiCA model, analyzing all possible linear rules, with the best and worst ReLiCA\* model, whose rules were selected by ReLiCADA. Best and worst are determined per dataset, resulting in the possibility that different rules are used for the different datasets. It can be seen that the best ReLiCA\* model is very close to the overall best ReLiCA model, especially considering that the overall worst rule has a mean  $NMSE > 1$ . Not only the best ReLiCA\* model shows nearly optimal performance, but also the worst one. It is also evident that increasing  $\hat{n}$  from 3 to 5 did not improve the performance. This behavior was also verified for several other values of  $m$  (see appendix C).

Instead of using only the mean  $NMSE$  for this analysis, we also checked how many ReLiCA models are worse than a selected ReLiCA\* model. The results are depicted in Fig. 12 and clearly show that the best ReLiCA\* model is at least better than 95% of the total rule space. Even the worst ReLiCA\* model is still better than 80% of the overall ReLiCA models. This again verifies that the performance of all rules selected by ReLiCADA is far better than randomly choosing a linear rule.

As it is reasonable to test all configurations selected by ReLiCADA it is possible to always achieve the best performance in Fig. 11 and 12.

Since one goal was to achieve a computationally simple model with low complexity while maintaining good model performance, we compared these two parameters in Fig. 13. We used a train-test-validation split of the dataset for this analysis. The test performance values were used to select the best model, and the validation performance values are shown in Fig. 13. No large deviations between test and validation performance were evident during our experiments. The ReLiCA models have less complexity compared to the RC and NN models. Despite their computational simplicity, they still achieve similar or even better performance. Increasing  $m$  for the ReLiCA models increases not only the model complexity but also the model performance. However, it is apparent that the performance gain by increasing  $m$  declines. A neighborhood of  $\hat{n} = 3$  was chosen for the ReLiCA models since increasing the neighborhood would not result in

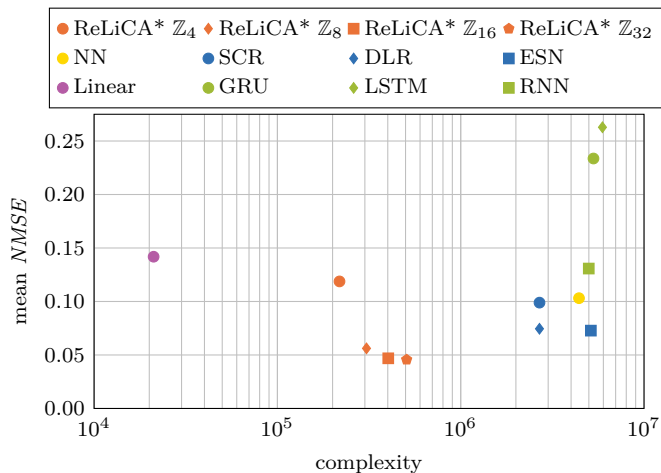


Fig. 13. Comparison of model performance with model complexity.

better performance.

Despite the nonlinear, and thus more complex, CA of the *Babson* models, their performance is not up to the ReLiCA\* models. While the ReLiCA\*  $\mathbb{Z}_4$  models achieve a mean *NMSE* of 0.12, the *Babson* models only achieve 0.34. As the nonlinear CA rules of the *Babson* models have been optimized with a GA, this indicates that heuristic search and optimization algorithms cannot deal with the structure and size of the general CA rule space very well.

To analyze the influence of the random mapping on the ReLiCA model performance, we tested several different seeds for the random mapping generator. While there is an influence on the performance, it is neglectable for the models selected by ReLiCADA. In Fig. 14, the empirical cumulative distribution function for different seeds is visualized for  $\mathbb{Z}_4$ ,  $\hat{n} = 3$  ReLiCA and ReLiCA\* models using *scale\_offset* and *replacement*. The slight performance difference decreases even further with larger  $m$ .

During our experiments, we mainly focused on the integer rings  $m = 2^a$  with  $a \in \mathbb{N}^+$  since these are most suitable for implementations on FPGAs and other digital systems. Nevertheless, we verified ReLiCADA for several other values of  $m$  (see appendix C). These results showed that ReLiCADA can also be used for  $m \neq 2^a$ . According to our experiments, CAs over  $\mathbb{Z}_2$  behave differently. For example, the best encoding for these CAs is the *xor* encoding. Since this configuration was not of primary interest, we did not analyze this further. Furthermore we verified ReLiCADA on lattice sizes not equal to (16,32) and iterations not equal to 4. Also, for these configurations, ReLiCADA showed great improvements in performance compared to the whole set of all possible ReLiCA models. The performance values are listed in appendix C.

We also ran tests where the quantized input  $x_q$  was directly fed into the readout layer, forming a quantized skip connection. When the *replacement* encoding was used, this did not lead to any performance gain. Since ReLiCADA only uses *replacement* encoding, quantized

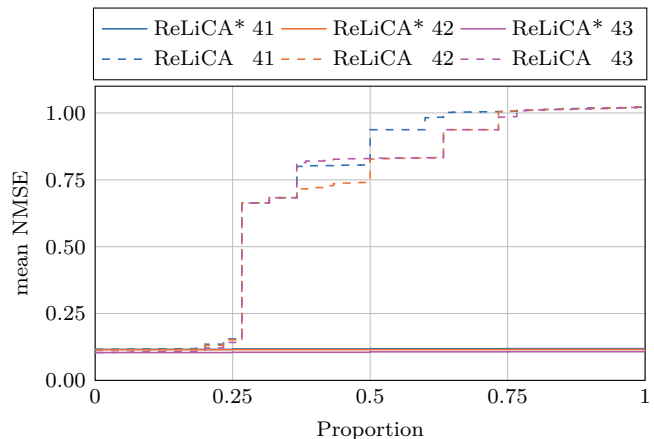


Fig. 14. Influence of the random mapping seed on the ReLiCA model performance. The used model configuration is:  $\mathbb{Z}_4$ ,  $\hat{n} = 3$ , *scale\_offset*, *replacement*.

skip-connections are not used in our models. However, a performance gain was observed when the readout layer was provided with the original input  $x$  directly. Since this imposes only a very little increase in complexity, we recommend using this skip connection if possible.

### C. Nonlinear Capabilities

During our experiments, we saw that ReLiCA models could not deal with highly nonlinear datasets, like *Hénon*, very well. However, after using the hyperparameter optimizer *Optuna* to optimize the quantization thresholds (see (35)) and the regularization of the Ridge optimizer, the performance of the ReLiCA model increased drastically. The ReLiCA\* model with  $\mathbb{Z}_{16}$ ,  $\hat{n} = 3$  achieved an *NMSE* of 0.321 before optimization and 0.048 after. Other transformation and quantization layers could likely improve the nonlinear capabilities of linear ReLiCA models. However, this was not further analyzed.

Further tests have shown that the ReLiCA model performance also improves on the other datasets when *Optuna* is used to optimize quantization thresholds. Since we wanted to create a fast and easy-to-train model, we refrained from using threshold optimization in our results.

## VII. CONCLUSION

ReCA represents a particular form of the broader field of RC that is particularly suited to be implemented on FPGAs. However, the choice of hyperparameters and, primarily, the search for suitable CA rules are major challenges during the design phase of such models. When restricted to linear CAs, fundamental properties can be computed analytically. Based on the results of nearly a million experiments, we recognized that linear CA rules that achieve low errors on many relevant benchmark datasets have specific mathematical properties. Based on these insights, we developed the Reservoir Computing using Linear Cellular Automata Design Algorithm, which selects hyperparameters that have been shown to work

well in the experiments. Most importantly, the proposed algorithm pre-selects a few rules out of the rule space that grows exponentially with increasing  $m$  and  $\hat{n}$ . As it has been shown, the best-performing selected rules are among the top 5% of the overall rule space. Moreover, the proposed models achieve, on average, a lower error than other state-of-the-art neural network models and, at the same time, exhibit less computational complexity, showing the strength of ReLiCADA. Furthermore, with the immensely reduced hyperparameter space, the time needed to design and implement ReCA models is drastically reduced. In conclusion, ReLiCADA is a promising approach for designing and implementing ReCA models for time series processing and analysis.

## APPENDIX A

### PERFORMANCE VALUES OF COMPARED MODELS

Tables II to IV list the  $NMSE$  values of the models compared throughout this paper. The dark blue color highlights the model with the lowest  $NMSE$  for the respective dataset. The light blue color indicates that the model has a similar performance (same value rounded to 3 decimal places) compared to the best model.

The validation performance values of the reference models are listed in Table II. All models except the Linear model were optimized using Optuna.

Tables III and IV list the performance values of the ReCA models for the test and validation set.

## APPENDIX B

### SUPPLEMENTARY MATERIALS

Supplementary files to this paper can be found in the git repository at <https://github.com/jkantic/ReLiCADA>.

## APPENDIX C

### PERFORMANCE VALUES OF RELICADA

The  $NMSE$  values of all tested ReLiCADA models are listed in the file *relicada\_performance.xlsx* (supplementary materials). The table lists the number of rules selected by ReLiCADA as well as the minimum, mean, and maximum  $NMSE$  values of the selected rules. If the whole rule space for a given configuration was tested, these values are also calculated for the whole set of rules. Furthermore, the percentage of rules worse than the best/worst ReLiCADA rule is stated.

## APPENDIX D

### TESTED CONFIGURATIONS

The file *configs.xlsx* (supplementary materials) contains all ReLiCA model configurations tested. The trans/quant column lists the used transformation and quantization algorithm.

## APPENDIX E

### RAW EXPERIMENT OUTPUT

The supplementary materials to this paper include CSV files containing the raw experiment results for all tested configurations. For each dataset, a separate CSV file lists:  $(N_r, N_c)$ ,  $I$ ,  $m$ ,  $\hat{n}$ , transformation, quantization, encoding, mapping, seed,  $\mathbf{w}$ , and the  $NMSE$  performance value.

## APPENDIX F

### RELICADA PSEUDOCODE

The pseudocode in algorithm 1 together with (43) to (46) and the explanation in section IV-B can be used to implement ReLiCADA.

## REFERENCES

- [1] G. Tanaka *et al.*, "Recent advances in physical reservoir computing: A review," *Neural Networks*, vol. 115, pp. 100–123, Jul. 2019.
- [2] K. Nakajima and I. Fischer, Eds., *Reservoir computing*. Springer Singapore, 2021.
- [3] H. Jaeger, "The "echo state" approach to analysing and training recurrent neural networks-with an erratum note," *Bonn, Germany: German National Research Center for Information Technology GMD Technical Report*, vol. 148, no. 34, p. 13, 2001.
- [4] D. E. Rumelhart, G. E. Hinton, and R. J. Williams, "Learning representations by back-propagating errors," *Nature*, vol. 323, no. 6088, pp. 533–536, Oct. 1986.
- [5] A. Rodan and P. Tino, "Minimum complexity echo state network," *IEEE Trans. Neural Netw.*, vol. 22, no. 1, pp. 131–144, Jan. 2011.
- [6] D. Verstraeten, B. Schrauwen, and D. Stroobandt, "Reservoir computing with stochastic bitstream neurons," in *Proceedings of the 16th annual Prorisc workshop*, 2005, pp. 454–459.
- [7] M. L. Alomar, V. Canals, N. Perez-Mora, V. Martínez-Moll, and J. L. Rosselló, "FPGA-based stochastic echo state networks for time-series forecasting," *Computational Intelligence and Neuroscience*, vol. 2016, pp. 1–14, 2016.
- [8] O. Yilmaz, "Reservoir computing using cellular automata," 2014.
- [9] M. Margem and O. Yilmaz, "How much computation and distributedness is needed in sequence learning tasks?" in *Artificial General Intelligence*. Springer International Publishing, 2016, pp. 274–283.
- [10] T. Natschläger and W. Maass, "Spiking neurons and the induction of finite state machines," *Theoretical Computer Science*, vol. 287, no. 1, pp. 251–265, Sep. 2002.
- [11] G.-B. Huang, Q.-Y. Zhu, and C.-K. Siew, "Extreme learning machine: Theory and applications," *Neurocomputing*, vol. 70, no. 1-3, pp. 489–501, Dec. 2006.
- [12] J. J. Steil, "Backpropagation-decorrelation: online recurrent learning with  $O(N)$  complexity," in *2004 IEEE International Joint Conference on Neural Networks (IEEE Cat. No. 04CH37541)*, vol. 2. Institute of Electrical and Electronics Engineers (IEEE), 2004, pp. 843–848.
- [13] J. von Neumann, "The General and Logical Theory of Automata," in *John von Neumann Collected Works*, A. H. Taub, Ed., vol. V. Pergamon Press, 1963, pp. 288–328.
- [14] J. von Neumann and A. W. Burks, *Theory of Self-Reproducing Automata*. University of Illinois Press, 1966.
- [15] W. Li and N. Packard, "The structure of the elementary cellular automata rule space," *Complex Systems*, vol. 4, pp. 281–297, 1990.
- [16] S. Wolfram, *A New Kind of Science*. Champaign, IL: Wolfram Media, 2002.
- [17] M. Itô, N. Ôsato, and M. Nasu, "Linear cellular automata over  $Z_m$ ," *Journal of Computer and System Sciences*, vol. 27, no. 1, pp. 125–140, Aug. 1983.
- [18] S. Wolfram, "Statistical mechanics of cellular automata," *Reviews of Modern Physics*, vol. 55, no. 3, pp. 601–644, Jul. 1983.



TABLE II  
BASELINE MODEL PERFORMANCE

	NN	RNN	GRU	LSTM	DLR	SCR	ESN	Linear
MG	0.000	0.001	0.001	0.001	0.000	0.000	0.000	0.000
MG_25	0.000	0.099	0.030	0.015	0.001	0.001	0.000	0.310
MSO	0.001	0.074	0.037	0.092	0.002	0.001	0.002	0.000
MSO_3	0.004	0.414	0.665	0.723	0.040	0.096	0.079	0.000
NARMA_10	0.021	0.107	0.627	0.403	0.062	0.055	0.116	0.161
NARMA_20	0.551	0.165	0.552	0.544	0.161	0.439	0.124	0.542
NARMA_30	0.544	0.449	0.542	0.538	0.545	0.488	0.476	0.536
NCC	0.002	0.018	0.033	0.455	0.007	0.006	0.002	0.010
PMP	0.000	0.000	0.000	0.001	0.000	0.000	0.000	0.000
PPST	0.000	0.002	0.001	0.022	0.000	0.000	0.000	0.000
PPST_10	0.010	0.109	0.084	0.097	0.002	0.002	0.002	0.000

TABLE III  
RECA MODEL PERFORMANCE (TEST-SET)

	Babson	ReLiCADA						
	$\mathbb{Z}_4$ $\hat{n} = 3$	$\mathbb{Z}_4$ $\hat{n} = 3$	$\mathbb{Z}_4$ $\hat{n} = 5$	$\mathbb{Z}_8$ $\hat{n} = 3$	$\mathbb{Z}_8$ $\hat{n} = 5$	$\mathbb{Z}_{16}$ $\hat{n} = 3$	$\mathbb{Z}_{16}$ $\hat{n} = 5$	$\mathbb{Z}_{32}$ $\hat{n} = 3$
MG	0.033	0.005	0.005	0.002	0.001	0.002	0.002	0.002
MG_25	0.052	0.018	0.013	0.004	0.004	0.008	0.008	0.034
MSO	0.510	0.112	0.113	0.029	0.029	0.008	0.008	0.002
MSO_3	0.647	0.129	0.129	0.033	0.031	0.009	0.009	0.002
NARMA_10	0.621	0.238	0.236	0.176	0.173	0.166	0.163	0.160
NARMA_20	0.649	0.204	0.204	0.145	0.145	0.134	0.135	0.131
NARMA_30	0.743	0.228	0.228	0.166	0.167	0.154	0.155	0.153
NCC	0.367	0.102	0.103	0.025	0.026	0.012	0.013	0.009
PMP	0.002	0.000	0.000	0.000	0.000	0.000	0.000	0.000
PPST	0.050	0.066	0.066	0.011	0.012	0.003	0.003	0.001
PPST_10	0.104	0.141	0.136	0.040	0.043	0.019	0.018	0.005

TABLE IV  
RELiCADA MODEL PERFORMANCE (VALIDATION-SET)

	$\mathbb{Z}_4$ $\hat{n} = 3$	$\mathbb{Z}_4$ $\hat{n} = 5$	$\mathbb{Z}_8$ $\hat{n} = 3$	$\mathbb{Z}_8$ $\hat{n} = 5$	$\mathbb{Z}_{16}$ $\hat{n} = 3$	$\mathbb{Z}_{16}$ $\hat{n} = 5$	$\mathbb{Z}_{32}$ $\hat{n} = 3$
MG	0.006	0.005	0.002	0.001	0.002	0.002	0.002
MG_25	0.018	0.016	0.004	0.004	0.010	0.010	0.036
MSO	0.115	0.120	0.031	0.030	0.008	0.008	0.002
MSO_3	0.137	0.138	0.034	0.034	0.009	0.010	0.002
NARMA_10	0.236	0.235	0.175	0.175	0.166	0.163	0.165
NARMA_20	0.179	0.182	0.130	0.130	0.120	0.119	0.118
NARMA_30	0.209	0.211	0.161	0.163	0.153	0.150	0.151
NCC	0.102	0.100	0.028	0.027	0.011	0.011	0.009
PMP	0.000	0.000	0.000	0.000	0.000	0.000	0.000
PPST	0.111	0.107	0.014	0.013	0.003	0.003	0.001
PPST_10	0.195	0.205	0.039	0.039	0.020	0.022	0.005

---

**Algorithm 1** ReLiCADA - Rule Selection
 

---

**Input:**  $N, m, \hat{n}$ **Output:** Selected rules  $S$ 

```

1:  $S \leftarrow \emptyset$ 
2:  $A \leftarrow \emptyset$ 
3:  $\mathcal{P}, \mathcal{K} \leftarrow \text{prime\_factors}(m)$   $\triangleright$  see (10) and (11)
4:  $\mathcal{P}_w, \bar{\mathcal{P}}_w \leftarrow \text{split\_ring}(m)$   $\triangleright$  see (12) and (13)
5: for each  $\mathbf{w} = (w_{-r}, \dots, w_r) \in \mathcal{R}(m, \hat{n})$  do  $\triangleright$  see (6)
6:    $A \leftarrow A \cup \{\mathbf{w}\}$ 
7:    $\hat{\mathbf{w}} = \text{mirror}(\mathbf{w})$ 
8:   if  $\hat{\mathbf{w}} \in A$  then
9:      $\triangleright$  see (43g)
10:    continue
11:  end if
12:   $\mathcal{H} \leftarrow \text{normalized\_entropy}(\mathcal{P}, \mathcal{K}, \mathbf{w})$   $\triangleright$  see (21)
13:  if  $\mathcal{H} \neq 1$  then
14:     $\triangleright$  see (43f)
15:    continue
16:  end if
17:  for each  $p \in \mathcal{P}$  do
18:     $P \leftarrow \{i : p \nmid w_i\}$ 
19:    if  $|P| \neq 1$  then
20:       $\triangleright$  see (43e)
21:      continue
22:    end if
23:  end for
24:  if  $\text{is\_prime}(m)$  then  $\triangleright \mathbb{Z}_m$  is a field
25:    if  $\exists w_i : (w_i \neq 0) \wedge (\mathcal{S}^\times(w_i) \neq \mathbb{Z}_m \setminus \{0\})$  then
26:       $\triangleright$  see (45)
27:      continue
28:    end if
29:  else if  $|\mathcal{P}| = 2$  then  $\triangleright \mathbb{Z}_m$  is a ring,  $m = p_1^{k_1} p_2^{k_2}$ 
30:     $\{p_1, p_2\} = \mathcal{P}$ 
31:    if  $(\forall w_i, w_j) : (p_1 \mid w_i) \vee (p_2 \mid w_j)$  then
32:       $\triangleright$  see (46)
33:      continue
34:    end if
35:  else  $\triangleright \mathbb{Z}_m$  is a ring
36:     $N \leftarrow \{i : w_i \neq 0\}$ 
37:    if  $|N| \neq 2$  then
38:       $\triangleright$  see (44a)
39:      continue
40:    end if
41:    if  $\exists w_i : (w_i \in \mathcal{P}_w) \wedge (w_i \notin \{1, m-1\})$  then
42:       $\triangleright$  see (44b)
43:      continue
44:    end if
45:    if  $m \neq 4$  then
46:      if  $\exists w_i : (w_i \in \bar{\mathcal{P}}_w) \wedge (|\mathcal{S}^+(w_i)| \neq 4)$  then
47:         $\triangleright$  see (44c)
48:        continue
49:      end if
50:    end if
51:  end if
52:   $S \leftarrow S \cup \{\mathbf{w}\}$ 
53: end for
54: return  $S$ 

```

---

- [19] O. Martin, A. M. Odlyzko, and S. Wolfram, "Algebraic properties of cellular automata," *Communications in Mathematical Physics*, vol. 93, no. 2, pp. 219–258, Jun. 1984.
- [20] A. K. Das, A. Sanyal, and P. Palchadhuri, "On characterization of cellular automata with matrix algebra," *Information Sciences*, vol. 61, no. 3, pp. 251–277, Jun. 1992.
- [21] B. Voorhees, "Additive cellular automata," in *Computational Complexity*. Springer New York, 2012, pp. 1–17.
- [22] M. A. Shereshevsky, "Lyapunov exponents for one-dimensional cellular automata," *Journal of Nonlinear Science*, vol. 2, no. 1, pp. 1–8, Mar. 1992.
- [23] L. P. Hurd, J. Kari, and K. Culik, "The topological entropy of cellular automata is uncomputable," *Ergodic Theory and Dynamical Systems*, vol. 12, no. 2, pp. 255–265, Jun. 1992.
- [24] J. Kari, "Reversibility and surjectivity problems of cellular automata," *Journal of Computer and System Sciences*, vol. 48, no. 1, pp. 149–182, Feb. 1994.
- [25] M. D'amico, G. Manzini, and L. Margara, "On computing the entropy of cellular automata," *Theoretical Computer Science*, vol. 290, no. 3, pp. 1629–1646, Jan. 2003.
- [26] D. Burguet, "Rescaled entropy of cellular automata," *Nonlinearity*, vol. 34, no. 7, pp. 4897–4922, Jun. 2021.
- [27] E. F. Codd, *Cellular Automata*, E. F. Codd, Ed. Academic Press, 1968.
- [28] N. H. Packard, "Adaptation toward the edge of chaos," *Dynamic Patterns in Complex Systems*, pp. 293–301, 1988.
- [29] C. G. Langton, "Computation at the edge of chaos: Phase transitions and emergent computation," *Physica D: Nonlinear Phenomena*, vol. 42, no. 1-3, pp. 12–37, Jun. 1990.
- [30] M. Mitchell, P. Hraber, and J. P. Crutchfield, "Revisiting the edge of chaos: evolving cellular automata to perform computations," 1993.
- [31] C. Teuscher, "Revisiting the edge of chaos: Again?" *Biosystems*, vol. 218, p. 104693, Aug. 2022.
- [32] J. Kari, "The nilpotency problem of one-dimensional cellular automata," *SIAM Journal on Computing*, vol. 21, no. 3, pp. 571–586, Jun. 1992.
- [33] S. Nichele and M. S. Gundersen, "Reservoir computing using nonuniform binary cellular automata," *Complex Systems*, vol. 26, no. 3, pp. 225–246, Oct. 2017.
- [34] S. Nichele and A. Molund, "Deep learning with cellular automaton-based reservoir computing," *Complex Systems*, vol. 26, no. 4, pp. 319–340, Dec. 2017.
- [35] H. Jaeger, "Adaptive nonlinear system identification with echo state networks," in *Proceedings of the 15th International Conference on Neural Information Processing Systems*, ser. NIPS'02. Cambridge, MA, USA: MIT Press, 2002, pp. 609–616.
- [36] N. Babson and C. Teuscher, "Reservoir computing with complex cellular automata," *Complex Systems*, vol. 28, no. 4, pp. 433–455, 2019.
- [37] M. Margem and O. S. Gedik, "Feed-forward versus recurrent architecture and local versus cellular automata distributed representation in reservoir computing for sequence memory learning," *Artificial Intelligence Review*, vol. 53, no. 7, pp. 5083–5112, Feb. 2020.
- [38] A. Moran, C. F. Frasser, M. Roca, and J. L. Rossello, "Energy-efficient pattern recognition hardware with elementary cellular automata," *IEEE Trans. Comput.*, vol. 69, no. 3, pp. 392–401, Mar. 2020.
- [39] T. E. Glover, P. Lind, A. Yazidi, E. Osipov, and S. Nichele, "The dynamical landscape of reservoir computing with elementary cellular automata," in *The 2021 Conference on Artificial Life*. MIT Press, 2021.
- [40] F. Mendivil and D. Patterson, "Dynamics of finite linear cellular automata over  $\mathbb{Z}_N$ ," *Rocky Mountain Journal of Mathematics*, vol. 42, no. 2, Apr. 2012.
- [41] E. Jen, "Linear cellular automata and recurring sequences in finite fields," *Communications in Mathematical Physics*, vol. 119, no. 1, pp. 13–28, Mar. 1988.
- [42] J. G. Stevens, "On the construction of state diagrams for cellular automata with additive rules," *Information Sciences*, vol. 115, no. 1-4, pp. 43–59, Apr. 1999.
- [43] K. Sutner, "Decomposition of additive cellular automata," *Complex Systems*, vol. 13, 2002.
- [44] X. Zhang and L. Hu, "Periods of polynomials over a galois ring," *Science China Mathematics*, vol. 56, no. 9, pp. 1761–1772, Mar. 2013.

- [45] C. Qureshi and D. Panario, "Rédei actions on finite fields and multiplication map in cyclic group," *SIAM Journal on Discrete Mathematics*, vol. 29, no. 3, pp. 1486–1503, Jan. 2015.
- [46] C. Qureshi and L. Reis, "Dynamics of the  $\alpha$ -map over residually finite Dedekind domains and applications," *Journal of Number Theory*, vol. 204, pp. 134–154, Nov. 2019.
- [47] R. Lidl and H. Niederreiter, *Finite fields*. Cambridge University Press, Oct. 1996.
- [48] D. S. Dummit, *Abstract Algebra*, R. M. Foote, Ed. Englewood Cliffs, NJ: Prentice-Hall, 1991.
- [49] D. Forney, *Principles of digital communication II*. Massachusetts Institute of Technology, 2005, ch. Introduction to finite fields.
- [50] S. Wolfram, "Random sequence generation by cellular automata," *Advances in Applied Mathematics*, vol. 7, no. 2, pp. 123–169, Jun. 1986.
- [51] G. Manzini and L. Margara, "A complete and efficiently computable topological classification of D-dimensional linear cellular automata over  $Z_m$ ," *Theoretical Computer Science*, vol. 221, no. 1-2, pp. 157–177, Jun. 1999.
- [52] G. Cattaneo, E. Formenti, G. Manzini, and L. Margara, "Ergodicity, transitivity, and regularity for linear cellular automata over  $Z_m$ ," *Theoretical Computer Science*, vol. 233, no. 1-2, pp. 147–164, Feb. 2000.
- [53] K. Butt, "An introduction to topological entropy," 2014.
- [54] B. J. LuValle, "The effects of boundary conditions on cellular automata," *Complex Systems*, vol. 28, no. 1, pp. 97–124, Mar. 2019.
- [55] B. Codenotti and L. Margara, "Transitive cellular automata are sensitive," *Amer. Math. Monthly*, vol. 103, no. 1, p. 58, Jan. 1996.
- [56] G. Cattaneo, E. Formenti, G. Manzini, and L. Margara, "On ergodic linear cellular automata over  $Z_m$ ," in *Lecture Notes in Computer Science*. Springer Berlin Heidelberg, 1997, pp. 427–438.
- [57] T. Sato, "Ergodicity of linear cellular automata over  $Z_m$ ," *Information Processing Letters*, vol. 61, no. 3, pp. 169–172, Feb. 1997.
- [58] R. L. Devaney, *A first course in chaotic dynamical systems*. Chapman and Hall/CRC, Apr. 2020.
- [59] G. H. Golub, P. C. Hansen, and D. P. O'Leary, "Tikhonov regularization and total least squares," *SIAM Journal on Matrix Analysis and Applications*, vol. 21, no. 1, pp. 185–194, Jan. 1999.
- [60] A. E. Hoerl and R. W. Kennard, "Ridge Regression: biased estimation for nonorthogonal problems," *Technometrics*, vol. 12, no. 1, pp. 55–67, Feb. 1970.
- [61] N.-Y. Liang, G.-B. Huang, P. Saratchandran, and N. Sundararajan, "A fast and accurate online sequential learning algorithm for feedforward networks," *IEEE Trans. Neural Netw.*, vol. 17, no. 6, pp. 1411–1423, Nov. 2006.
- [62] D. Verstraeten, J. Dambre, X. Dutoit, and B. Schrauwen, "Memory versus non-linearity in reservoirs," in *The 2010 International Joint Conference on Neural Networks (IJCNN)*. Institute of Electrical and Electronics Engineers (IEEE), Jul. 2010, pp. 1–8.
- [63] G. Cattaneo, E. Formenti, and L. Margara, "Topological definitions of deterministic chaos," in *Cellular Automata*. Springer Netherlands, 1999, pp. 213–259.
- [64] M. Hénon, "A two-dimensional mapping with a strange attractor," *Communications in Mathematical Physics*, vol. 50, no. 1, pp. 69–77, Feb. 1976.
- [65] M. Mackey and L. Glass, "Oscillation and chaos in physiological control systems," *Science (New York, N.Y.)*, vol. 197, no. 4300, pp. 287–289, Jul. 1977.
- [66] A. Esposito, M. Faundez-Zanuy, F. C. Morabito, and E. Pasero, Eds., *Neural advances in processing nonlinear dynamic signals*. Springer International Publishing, 2019.
- [67] A. F. Atiya and A. G. Parlos, "New results on recurrent network training: unifying the algorithms and accelerating convergence," *IEEE Trans. Neural Netw.*, vol. 11, no. 3, pp. 697–709, May 2000.
- [68] H. Chen, F. Tang, P. Tino, and X. Yao, "Model-based kernel for efficient time series analysis," in *Proceedings of the 19th ACM SIGKDD international conference on Knowledge discovery and data mining*. ACM, Aug. 2013.
- [69] H. Jaeger and H. Haas, "Harnessing nonlinearity: predicting chaotic systems and saving energy in wireless communication," *Science*, vol. 304, no. 5667, pp. 78–80, Apr. 2004.
- [70] D. Dua and C. Graff, "UCI machine learning repository," 2017. [Online]. Available: <http://archive.ics.uci.edu/ml>
- [71] S. Park, D. Lee, and W. W. Chu, "Fast retrieval of similar subsequences in long sequence databases," in *Proceedings 1999 Workshop on Knowledge and Data Engineering Exchange (KDEX'99) (Cat. No. PR00453)*. Institute of Electrical and Electronics Engineers (IEEE), 1999.
- [72] Y. Xue, L. Yang, and S. Haykin, "Decoupled echo state networks with lateral inhibition," *Neural Networks*, vol. 20, no. 3, pp. 365–376, Apr. 2007.
- [73] M. Abadi *et al.*, "TensorFlow: Large-scale machine learning on heterogeneous systems," 2015, software available from tensorflow.org. [Online]. Available: <https://www.tensorflow.org/>
- [74] D. P. Kingma and J. Ba, "Adam: A method for stochastic optimization," 2014.
- [75] K. Cho *et al.*, "Learning phrase representations using RNN encoder-decoder for statistical machine translation," 2014.
- [76] S. Hochreiter and J. Schmidhuber, "Long short-term memory," *Neural Computation*, vol. 9, no. 8, pp. 1735–1780, Nov. 1997.
- [77] F. Rosenblatt, "The perceptron: A probabilistic model for information storage and organization in the brain," *Psychological Review*, vol. 65, no. 6, pp. 386–408, 1958.
- [78] F. Pedregosa *et al.*, "Scikit-learn: Machine Learning in Python," *Journal of Machine Learning Research*, vol. 12, pp. 2825–2830, 2011.
- [79] T. Akiba, S. Sano, T. Yanase, T. Ohta, and M. Koyama, "Optuna: A next-generation hyperparameter optimization framework," in *Proceedings of the 25th ACM SIGKDD International Conference on Knowledge Discovery & Data Mining*. ACM, Jul. 2019.
- [80] H. S. Wall, *Analytic theory of continued fractions*. D. Van Nostrand Company, 1948. [Online]. Available: <https://archive.org/details/dli.ernet.16804>